mater.scichina.com link.springer.com

Published online 19 October 2022 | https://doi.org/10.1007/s40843-022-2197-4
Sci China Mater 2023, 66(1): 1–21

Flexible perovskite light-emitting diodes: Progress, challenges and perspective

Jin-Tao Wang[1], Shu-Zhuang Wang[1], Yu-Hang Zhou[1], Yan-Hui Lou[2*] and Zhao-Kui Wang[1*]

ABSTRACT **Metal halide perovskites with excellent optoelectronic properties and good ductile properties have emerged as promising materials suitable for flexible optoelectronics that can be integrated into portable and wearable display devices, showing great potential for the next generation displays and lighting. Currently, encouraging progress has been witnessed in the field of flexible perovskite light-emitting diodes (PeLEDs), with maximal external quantum efficiencies (EQEs) of over 28%. Herein, we summarize the major breakthroughs in recent years, with the aim of providing a comprehensive review and facilitating the further development of flexible PeLEDs. In addition, the main challenges that hinder the performance and commercialization of flexible PeLED devices are discussed. Finally, a brief perspective and conclusion toward the future opportunities and applications of flexible PeLEDs are provided.**

Keywords: metal halide perovskites, perovskite light-emitting diodes, flexible optoelectronics

INTRODUCTION

With the continuous advancement of science and technology, flexible, portable, and wearable electronic devices have attracted widespread attention, which are required in human-computer interaction interfaces. As the main window of receiving information, the quality of the display directly determines the users' experience. Therefore, the development of ultra-thin, lightweight, flexible, and high-color purity light-emitting diodes (LEDs) is of great significance for the next generation of lighting and display technologies [1]. Among all the light-emitting materials, metal halide perovskites (MHPs) have become a "rising star" owing to their excellent optical and electrical properties, such as high photoluminescence quantum yield (PLQY), high color purity, wide color gamut, and solution processibility [2–5]. Since the naissance of the room-temperature electroluminescent perovskite LEDs (PeLEDs) in 2014, PeLEDs have undergone rapid development [6–10]. So far, the external quantum efficiencies (EQEs) of rigid PeLEDs have recorded 28.1% and 22.2% for green and near-infrared (NIR) PeLEDs, respectively [11,12], which are comparable to conventional organic LEDs (OLEDs). However, rigid PeLEDs are incompatible with the demand for flexible electronics due to their weaknesses of rigidity, fragility, and heavy-weight [13].

In order to meet the practical applications of flexible devices, each functional layer of the flexible PeLEDs (i.e., bottom electrodes, hole-transporting layers (HTLs), perovskite emission layers, electron-transporting layers (ETLs), and top electrodes) should have prominent mechanical properties such as good flexibility and stability. In theory, due to the inherent flexibility and ductility of MHPs and the same operating principle of flexible and rigid PeLEDs [14,15], flexible PeLEDs can be achieved by replacing rigid substrates (e.g., indium tin oxide (ITO)) and electrodes with flexible transparent substrates and electrodes (e.g., metal nanowires (NWs), graphene, carbon nanotubes (CNTs), and conducting polymers). The first flexible PeLED was reported by Kim *et al.* [16] in 2014 by simply replacing the rigid ITO-glass substrate with the flexible plastic substrate. The EQE was only 0.125%. Since then, the pursuit of high-performance and high-flexibility PeLEDs has become a research hotspot in the field of MHPs-based optoelectronics. In 2017, Seo *et al.* [17] used graphene instead of ITO as the anode to effectively reduce the exciton quenching. Furthermore, due to the soft nature of graphene, they prepared flexible PeLEDs on polyethylene terephthalate (PET) substrates, achieving the highest EQE of 3.8%. Cheng *et al.* [18] adopted a di-additive strategy to remarkably improve the morphology of perovskite films, and obtained flexible PeLEDs with the champion EQE of 10.1%. Zhao *et al.* [19] developed a new hole-transporting material with shallower ionization potential, which successfully improved the charge balance. Finally, they fabricated high-efficiency and large-area flexible PeLEDs with a maximum EQE of 12.1%. In 2020, Shen *et al.* [20] proposed rational interface engineering, effectively passivating the defects, and suppressing the nonradiative recombination loss. As a result, in combination with appropriate light outcoupling nanostructures, they achieved the highest EQE of 24.5%, which is so far the most advanced value in the research community of flexible PeLEDs.

For an ideal flexible PeLED with high performance, the figures of merit could be divided into two groups, namely device performance parameters and flexible performance parameters. The key device performance parameter is the EQE, which is defined as the proportion of emitted photons to the number of electrons injected into the device and can be calculated by the equation: $EQE = IQE \times \eta_{oc}$, where IQE is the internal quantum efficiency, defined as the number of electron-hole pairs generated per absorbed photon; and η_{oc} is the light outcoupling efficiency, defined as the ratio of generated photons in the emissive layer

[1] Institute of Functional Nano & Soft Materials (FUNSOM), Jiangsu Key Laboratory for Carbon-Based Functional Materials & Devices, Soochow University, Suzhou 215123, China
[2] College of Energy, Soochow Institute for Energy and Materials Innovations, Soochow University, Suzhou 215006, China
* Corresponding authors (emails: zkwang@suda.edu.cn (Wang ZK); yhlou@suda.edu.cn (Lou YH))

that exit the device [21,22]. Moreover, other key quality factors also include the brightness L (cd m^{-2}) and the current efficiency CE (cd A^{-1}) [21]. For the flexibility performance, the main parameters include the bending radius or radius of curvature, bending angle, and tensile strains. Usually, to test the flexibility of the devices, the flexible PeLEDs could be used to perform a cyclic bending test at a certain bending radius or bending angle and then collect the performance after different bending cycles. Finally, the flexibility performance will be reflected by the degradation of the device performance such as EQE and brightness.

There is no doubt that the perovskite emitting layer plays a decisive role in the performance of flexible PeLEDs. Nevertheless, proper optimization of other functional layers is also essential to further improve the device performance. On this basis, we comprehensively summarize the recent progress in flexible PeLEDs, starting with the introduction of flexible PeLEDs and mainly focusing on the reported optimization strategies for every single functional layer. Afterward, the main current challenges of flexible PeLEDs are discussed in terms of stability, mechanical robustness, luminescence chromaticity balance, toxicity, and large-area fabrication. Finally, the future research directions of flexible PeLEDs are prospected. Fig. 1 gives an illustration of the roadmap for this review.

FLEXIBLE PEROVSKITE LEDs

In this section, the fundamentals of flexible PeLEDs including the crystal structure and physical properties of perovskite materials, working mechanisms of PeLEDs, as well as special materials suitable for each functional layer of flexible PeLEDs are summarized.

Perovskite materials

Over the past several years, MHPs have been intensively investigated as a promising luminescent material due to their excellent optoelectronic properties suitable for light-emitting applications, such as high PLQY, narrow emission width, high absorption coefficient, tunable bandgap, and high charge carrier mobility [2,25,26]. The general molecular formula of the three-dimensional (3D) perovskites is ABX_3, where the A-site represents a monovalent organic or inorganic cation (e.g., $CH_3NH_3^+$ (MA^+), $CH(NH_2)_2^+$ (FA^+), and Cs^+), the B-site is occupied by a divalent metal cation such as Pb^{2+} and Sn^{2+}, and the X-sites are halide anions (e.g., Cl^-, Br^-, and I^-), as shown in Fig. 2a. The Goldschmidt tolerance factor (t) and octahedral factor (μ) can be considered as criteria to estimate the crystallographic stability and formation possibility of perovskite structures given by the following formulas:

$$t = \frac{R_A + R_B}{\sqrt{2}(R_B + R_X)}, \quad (1)$$

$$\mu = \frac{R_B}{R_X}, \quad (2)$$

where R_A, R_B, and R_X represent the ionic radii of A, B, and X ions, respectively [27,28]. Generally, the typical 3D perovskites can be formed when $0.80 < t < 0.90$ and $0.40 < \mu < 0.90$ [21,29]. For halide perovskites, the factors are usually in the range of $0.81 < t < 1.11$ and $0.44 < \mu < 0.90$ [28].

Usually, the PL peaks can be tuned from 400 to 700 nm covering the entire visible spectra by varying the composition and ratio of halides in $MAPbX_3$ or $CsPbX_3$ nanocrystals (NCs) [24,30]. Fig. 2b shows the PL emission spectra of $CsPbX_3$ NCs where the X anion ranges from Cl to Br to I, with a narrow full

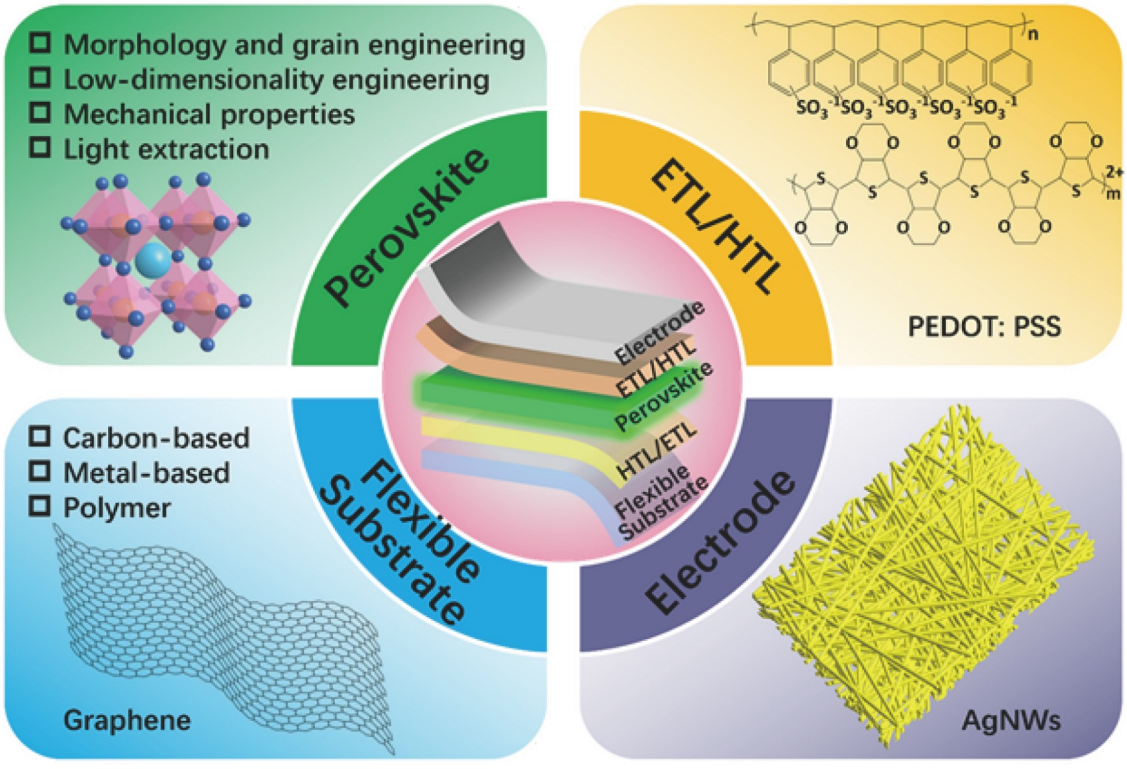

Figure 1 Illustration of the roadmap of this review, including the optimization strategies and some commonly used materials for various functional layers of the flexible PeLEDs.

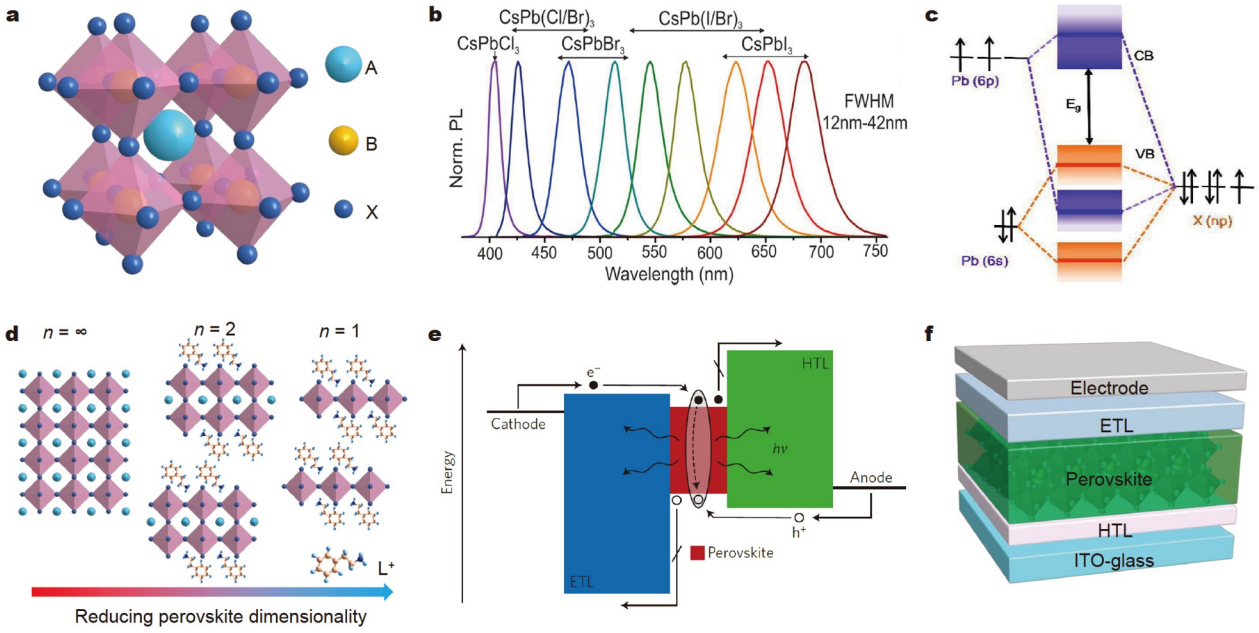

Figure 2 (a) Schematic representation of the perovskite crystal structure. (b) The tunable emission wavelength of colloidal $CsPbX_3$ (X = Cl, Br, I) NCs covering the full visible region. Reprinted with permission from Ref. [23]. Copyright 2015, American Chemical Society. (c) Schematic illustration of the energy band orbitals of $APbX_3$ perovskites. Reprinted with permission from Ref. [24]. Copyright 2016, American Chemical Society. (d) The dimensionality of MHPs. (e) Schematic illustration of the working principle of PeLEDs. Reprinted with permission from Ref. [3]. Copyright 2016, Springer Nature. (f) Schematic device diagram of a typical rigid PeLED architecture.

width at half maximum (FWHM) in the range of 12 to 42 nm [23]. It is noteworthy that mixed Cl/I perovskite NCs cannot be successfully synthesized because of the significant difference in ionic radii. This halide-dependent tunable emission can be attributed to the modification of band-edge states caused by the hybridization of the s-orbitals and p-orbitals of the halogen anions and B-site cations [31]. A simplified schematic diagram of the bonding (σ) and antibonding (σ*) orbitals in $CsPbX_3$ demonstrating the formation of energy bands is shown in Fig. 2c [24]. The conduction band minima (CBM) of MHPs are reported to consist mainly of the anti-bonding hybridization of Pb 6p and X *n*p (Cl: $n = 3$, Br: $n = 4$, I: $n = 5$) orbitals, with the main contribution coming from the Pb 6p orbitals, while the valance band maxima (VBM) are caused by the overlap of Pb 6s and X *n*p orbitals, with the X *n*p orbitals dominating. When the composition of the X-site changes from Cl to Br and then to I, the energies of X *n*p orbitals will increase accordingly, leading to a shift of the VBM to a shallower potential [24,32,33]. By introducing large organic cations into the 3D perovskite frameworks, 2D or quasi-2D perovskites with the formula of $L_mA_{n-1}B_nX_{3n+1}$ (L^+ is the large organic divalent cation with $m = 1$ or monovalent cation with $m = 2$; n is the number of metal halide octahedral sheets between L^+ cations; $n = 1$: 2D perovskites; n = defined integer: quasi-2D perovskites; and $n = \infty$: 3D perovskites) and perovskite quantum dots (QDs) can be obtained, as shown in Fig. 2d [2,34]. Beneficial from the enhanced quantum effect and dielectric confinement effect, these low-dimensional counterparts possess high radiative recombination efficiency [35,36].

Working mechanism of PeLEDs

The working mechanism of PeLEDs is shown in Fig. 2e, where the perovskite emission layer is sandwiched between the ETL and HTL [3]. Under forward bias, the carriers (i.e., electrons and holes) from the electrodes (i.e., cathode and anode) will be injected into the thin perovskite luminescent layer through the ETL and HTL, respectively. Then, the electrons and holes will recombine in a radiative manner, generating light (photons) in all directions [3,37]. During this light emission process, non-radiative recombination such as Auger recombination may happen, aggravating energetic losses and efficiency reduction [14]. Therefore, how to optimize the charge-transport characteristics (e.g., carrier injection and accumulation) of the perovskite emissive layers is essential to achieve high-performance PeLEDs [21]. The typical device architecture of a rigid PeLED is shown in Fig. 2f.

Flexible PeLEDs

Compared with inorganic materials, MHPs are much softer, which could be attributed to the high degree of anisotropy, low shear modulus, and low mechanical hardness of crystals [14]. Due to their good mechanical properties, MHPs have been regarded as potential materials suitable for flexible and stretchable devices, wearable displays, and biomedical devices [38–40].

The good ductile properties of MHPs can be mainly attributed to the A-site cations, bonding between metal and halide ions (B–X bonding), and the polycrystalline film of MHPs [14]. Nowadays, the effect of A-site organic cations on the mechanical properties of MHPs is still controversial. Most researchers believe that the soft properties of MHPs are strongly influenced by the A-site cations [14], while some reports also suggested that the A-site cations might only provide an equilibrium charge and fill the cavity between the framework of Pb and halides [41]. Furthermore, some researchers demonstrated by the *ab initio* molecular dynamics (AIMD) calculations that the A-site organic cation might only contribute to the strength and configuration

of the B–X bonding [42]. In contrast, it is believed that the inorganic backbone between the metal cations and halides (B–X) plays a more important role in the mechanical properties. The mechanical properties of the B–X framework are primarily influenced by the bonding strength and flexibility of the B–X bonding. Therefore, the electronegativity of halides also plays a significant part in influencing the mechanical stiffness of the B–X framework [38]. As the electronegativity (E) decreases from Cl to Br to I, the Young's modulus is measured in the order of $E_{Cl} > E_{Br} > E_I$, which is further confirmed by the first-principles density functional theory (DFT) calculations [15]. In addition, molecular dynamics simulations demonstrated that the single-crystalline perovskite films have more stiffness and higher tensile strength than the polycrystalline perovskite films [43].

After discussing the mechanical properties of MHPs, we do believe that the application of MHPs materials in flexible devices is tremendously feasible. Theoretically, flexible PeLEDs can be easily obtained by converting the functional layers in rigid PeLEDs into flexible layers, especially the rigid substrates and electrodes. Fig. 3a shows the typical structure of the flexible PeLEDs, with flexible conducting substrates (e.g., PET [46], polyethylene naphthalate (PEN) [47]) and flexible electrodes (e.g., AgNWs [48], graphene [17], CNTs [49]). The energy level data for the most common materials used as ETLs, HTLs, and perovskite emission layers are summarized in Fig. 3b [13,44,45].

PROGRESS IN FLEXIBLE PeLEDs

In this section, the recent progress in flexible PeLEDs, focusing on various functional layers including perovskite emissive layers, charge transporting layers (CTLs), flexible electrodes, and substrates, is discussed in sequence.

Perovskite emission layer

Morphology and grain engineering

It is believed that the surface morphology and grain size distribution of the perovskite films play a crucial role in the performance of flexible PeLEDs since the quality of perovskite films significantly affects the optoelectrical properties, mechanical properties, and device performance of PeLEDs [50–52]. Furthermore, good film morphology and uniform grain size distribution are prerequisites for maximizing the radiative recombination [14]. To obtain uniform and compact perovskite films, feasible strategies such as additive engineering [11,52,53], crystallization process controlling [54,55], and material composition management [56] have been successfully demonstrated. Cheng *et al.* [18] demonstrated a special dual-additive strategy to synergistically control the morphology of perovskite films. Firstly, they introduced phenethylammonium bromide (PEABr) to partially replace Cs^+ at grain boundaries to impede the growth of perovskites and partially convert 3D $CsPbBr_3$ perovskites to 2D structures, forming mixed-dimensional phases, which were characterized by small grain sizes and efficient energy funneling [35,57]. Meanwhile, another additive, dielectric polyethyleneglycol (PEG) was incorporated into the $CsPbBr_3$ precursor to enhance the homogeneity of the perovskite films, passivate the grain surface, and reduce the defect density through strong chemical interaction with $CsPbBr_3$ [58]. The schematic mechanism is shown in Fig. 4a. Fig. 4b shows the scanning electron microscopy (SEM) images of the morphologies of the perovskite films. Compared with the $CsPbBr_3$ perovskite film, the "$CsPbBr_3$ + PEG + PEABr" film was denser and had fewer pinholes. Based on this synergetic morphology con-

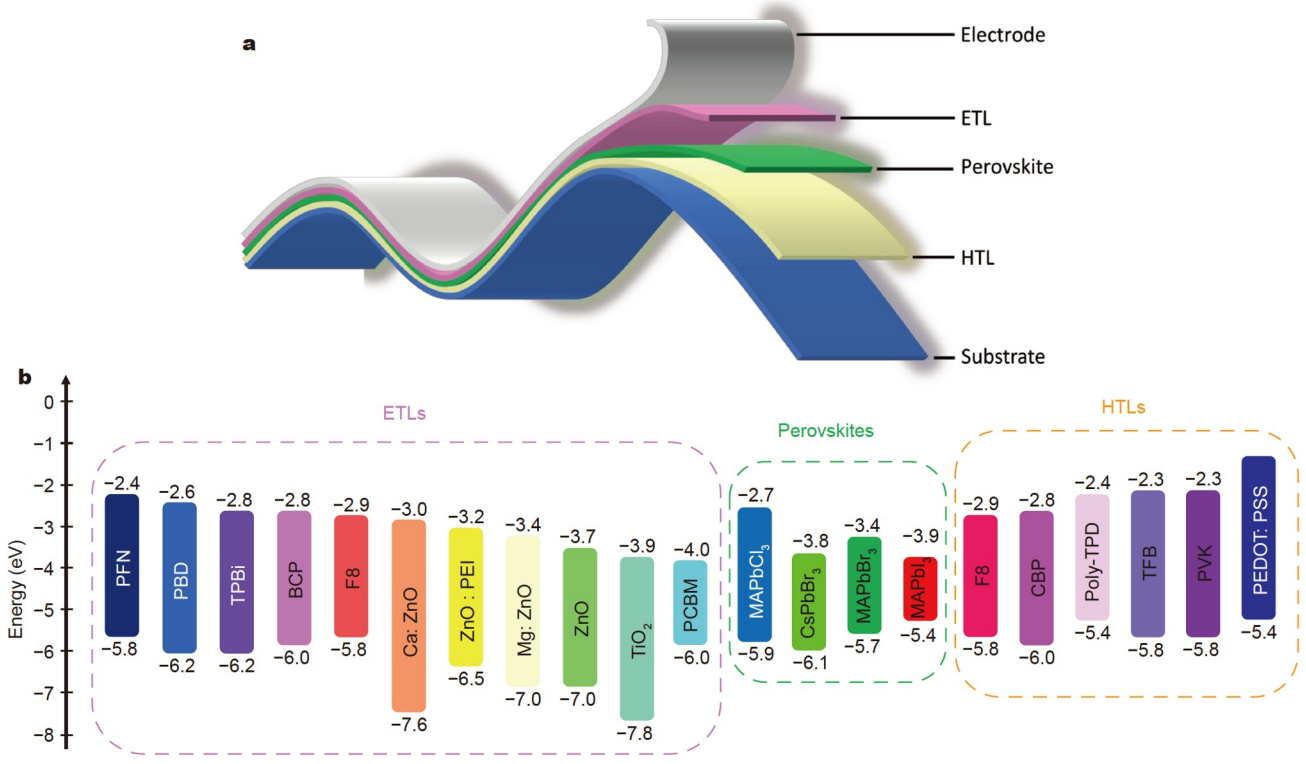

Figure 3 (a) Schematic illustration of the general flexible PeLEDs device architecture. (b) Energy level diagram of some commonly used ETLs, emission perovskites, and HTLs. The values of energy levels were collected from Refs [13,44,45].

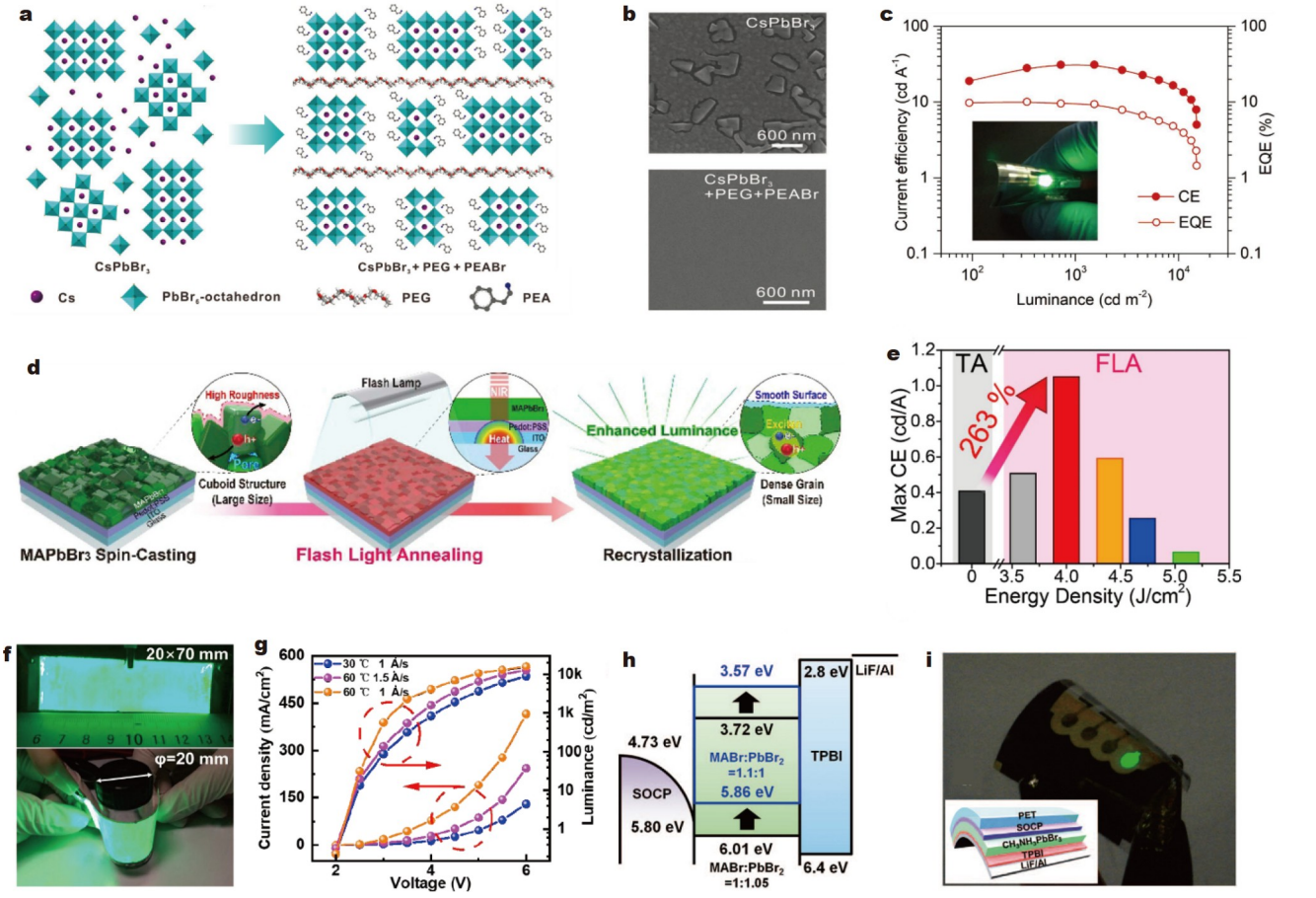

Figure 4 (a) Schematic mechanism of the synergetic morphology control with two additives including PEABr and PEG. (b) SEM images of $CsPbBr_3$ perovskite films with the incorporation of PEABr and PEG. (c) The current efficiency and EQE *versus* luminance curves of the flexible PeLEDs. The inset image is the optical photograph of a flexible PeLED. Reprinted with permission from Ref. [18]. Copyright 2018, Wiley-VCH. (d) Schematic illustration of the FLA method used for ultrafast recrystallization of perovskite films. (e) Comparison of the maximum current efficiencies of the PeLEDs with thermal annealing and FLA treatment. Reprinted with permission from Ref. [55]. Copyright 2019, Elsevier Ltd. (f) Photographs of a large-scale (70 mm × 20 mm) flexible green-emitting PeLED. (g) The current density and luminance curves as a function of voltage at different substrate temperatures and deposition rates. Reprinted with permission from Ref. [54]. Copyright 2020, American Chemical Society. (h) Energy band diagram of the PeLEDs, showing a decrease in ionization energy with increasing MABr molar ratio. (i) Photograph of a flexible PeLED on a PET substrate. Inset: the device structure of the flexible PeLEDs. Reprinted with permission from Ref. [56]. Copyright 2015, American Association for the Advancement of Science.

trol, researchers fabricated rigid PeLEDs with the maximal brightness of 45,990 cd m^{-2} and a champion EQE of 13.14%. Furthermore, flexible PeLEDs with the structure of PET/poly-(3,4-ethylenedioxythiolhene):poly(styrene sulfonate) (PEDOT:PSS)/$CsPbBr_3$/2,2′,2″-(1,3,5-benzenetriyl) tris-[1-phynyl-1*H*-ben-zimidazole] (TPBi)/LiF/AgNWs were prepared. The photograph of a flexible device is shown in the inserted image in Fig. 4c. As shown in Fig. 4c, the flexible PeLEDs exhibited excellent device performance with a peak EQE of 10.1% and a current efficiency of 31.0 cd A^{-1}. In addition, the crystallization is also a key process to control the morphology of perovskite films. Jung *et al.* [55] innovatively reported a flash light annealing (FLA) method to recrystallize $MAPbBr_3$ perovskites. Fig. 4d shows the schematic diagram of the recrystallization process *via* the FLA method. It can be clearly seen that the perovskite film had a cuboidal morphology after the spin-casting, leading to large roughness and lots of voids; while after the treatment of a xenon flash lamp to induce the recrystallization of $MAPbBr_3$ perovskites without photothermic damage, which was so-called FLA, the surface of the perovskite film was smoother and the grain size is smaller. At the same time, the luminance was significantly enhanced. Based on this unique annealing method, they fabricated high-performance flexible PeLEDs. Compared with the conventional thermally annealed flexible devices, the current efficiency and luminance of the FLA-treated devices were increased by 263% and 409%, respectively, as shown in Fig. 4e. Meanwhile, Chen *et al.* [54] also investigated the crystallization process. They demonstrated an *in-situ* dynamic thermal crystallization, in which thermal co-evaporation and successive low-temperature thermal annealing were employed to tune the morphology of perovskite films. Through tuning the substrate temperature and deposition rate, optimal rigid PeLEDs with a maximum EQE of 3.26% and a brightness of ~17,350 cd m^{-2} were realized. In addition, the current efficiency of the PeLEDs was as high as ~10.3 cd A^{-1}. Furthermore, by precisely adjusting the substrate temperature (60 ± 1°C) and deposition rate (1.0 Å s^{-1}), researchers successfully fabricated flexible PeLEDs with a large area (70 mm × 20 mm) as shown in Fig. 4f. These large-scale flexible PeLEDs showed excellent device performance with a high luminance of ~10,000 cd m^{-2} and an optimal current density of ~400 mA cm^{-2}, as shown in Fig. 4g. The fabrication method they proposed provided a viable

solution to facilitate the development of large-area flexible perovskite optoelectronic devices.

Cho *et al.* [56] reported high-performance flexible green PeLEDs through material composition control and grain engineering. In terms of the compositional control, by increasing the ratio of methylammonium bromide (MABr), researchers suppressed the generation of metallic Pb defects, and thus decreased the radiative recombination [59]. Meanwhile, the ionization energy decreased from 6.01 to 5.86 eV with the ratio of MABr and $PbBr_2$ increasing from 1:1.05 to 1.1:1, as illustrated in Fig. 4h. And the average grain size of $MAPbBr_3$ film was reduced to 99.7 nm through the NC pinning process. As a result, the excitons were spatially confined and the measured carrier diffusion length was 67 nm, leading to enhanced radiative recombination [5]. Finally, high-performance PeLEDs on rigid ITO substrate with the best EQE of 8.53% and current efficiency of 42.9 cd A^{-1} were realized. Using PET as the flexible substrate and a self-organized conducting polymer (SOCP) which consisted of PEDOT:PSS and a perfluorinated ionomer, tetrafluoroethylene-perfluoro-3,6-dioxa-4-methyl-7-octenesulfonic acid copolymer (PFI) and a small quantity of dimethyl sulfoxide (DMSO) as an additive, served as both anode and hole injection layer, flexible PeLEDs were successfully obtained. Fig. 4i depicts the device structure and photo of a flexible PeLED. This highly efficient flexible PeLED based on composition control and grain engineering exhibited good operation stability even in the high bending state.

Low-dimensionality engineering

Typical 3D perovskites have excellent optoelectrical properties such as low exciton binding energies and high dielectric constants, as well as long diffusion lengths, which are suitable for solar cells (SCs) [60–63]. However, these properties hinder the radiative recombination of charge carriers, leading to the lower radiative efficiency in PeLEDs [63]. Although the aforementioned grain engineering could accelerate the radiative recombination by reducing the grain size, it might destabilize the PeLEDs [64]. Another approach to improve the performance of PeLEDs is to reduce the dimensionality of MHPs by introducing 2D perovskites, quasi-2D perovskites, or perovskite QDs [21,44]. As previously mentioned, low dimensional perovskites with a general formula of $(RNH_3)_2A_{n-1}M_nX_{3n+1}$ could be formed by introducing large cations L^+. Both 2D and quasi-2D perovskites possess natural quantum-well structures, which could induce strong dielectric confinement and quantum confinement effects [65–68]. As a result, the radiative recombination, PLQY values, and PL intensity could be enhanced significantly [69,70]. In addition, perovskite QDs with superior optical properties are also considered as promising lighting materials [71].

The first PeLEDs based on 2D perovskites were demonstrated by Liang *et al.* [72]. They prepared high-quality 2D perovskite nanoplates and achieved blue PeLEDs with an electroluminescence (EL) peak at 410 nm and an EQE of 0.04% at room temperature. Kumar *et al.* [73] demonstrated ultrapure green PeLEDs based on colloidal 2D $FAPbBr_3$ perovskites. The 2D phase nature of $FAPbBr_3$ perovskites was confirmed by X-ray diffraction (XRD) and grazing-incidence wide-angle X-ray scattering (GIWAXS) measurements, as shown in Fig. 5a. The main peaks at 15°, 30°, and 45° in the XRD spectra corresponded to the lattice planes of (100), (200), and (300), respectively. The calculated 2D $MAPbBr_3$ and $FAPbBr_3$ perovskites lattice constants were 5.9 and 6.0 Å, respectively. And the Debye-Scherrer ring for the (100) plane in the GIWAXS pattern was in line with the XRD measurement. Fig. 5b shows the temperature-dependent PL curves. Through the dielectric quantum well engineering, the exciton binding energy of the perovskite films was increased to 161.6 meV with a PLQY as high as 92%. Additionally, they fabricated ultra-flexible PeLEDs on flexible polyimide (PI) substrates with the device structure of PI/ITO/PEDOT:PSS/poly(*N*,*N*′-bias(4-butyl phenyl)-*N*,*N*′-biphenyl benzidine) (poly-TPD)/$FAPbBr_3$-polymethyl methacrylate (PMMA)/tris(2,4,6-trimethyl-3-(pyridin-3-yl)phenyl)borane (3TPYMB)/LiF/Al. The photographs of the flexible PeLEDs are shown in the inset images in Fig. 5c. The flexible PeLEDs with an EL peak at 530 nm exhibited a maximal current efficiency of 8.4 cd A^{-1} and a maximum EQE of 2.0%. In addition, the researchers tested the flexibility of the devices. The flexible devices realized a minimum bending radius of 2 mm, and the devices could work even at a radius of 7.5 mm. As for quasi-2D PeLEDs, numerous reports have investigated systematically with the recorded EQEs of more than 21% on rigid glass substrates [74,75]. There are also many representative examples of flexible PeLEDs based on quasi-2D perovskites. Zhao *et al.* [76] demonstrated high-performance flexible PeLEDs based on quasi-2D perovskites with a peak EQE of 13%. Bade *et al.* [49] prepared flexible PeLEDs with fully-printed quasi-2D perovskite as the emitting layer, and the device structure was polymer substrate/CNTs/polyethylene oxide (PEO)/quasi-2D perovskite/AgNWs. The flexible devices showed good performance with a maximum brightness of 360 cd m^{-2}, an improvement of 256%.

More recently, Zhang *et al.* [77] proposed a general growth method, namely close-spaced vapor reaction (CSVR) for growing large-area and high-uniformity arrays of polycrystalline $MAPbBr_3$ perovskite quantum wires (QWs). Fig. 5d shows the schematic diagrams of the growth of perovskite QWs *via* the CSVR method. Firstly, $MAPbBr_3$ perovskites grew through the holes of hydrophobic alumina membranes (PAMs) until the overgrowth without visible PL. Then, the polycrystalline perovskite film on the surface was removed by ion milling. Finally, perovskite QWs arrays with high uniformity could be formed. By adjusting the diameter of holes in PAMs, perovskite QWs with different diameters could be grown. As can be seen in Fig. 5e, as the quantum well diameter decreased from 280 to 6.4 nm, the PLQY values of the $MAPbBr_3$ films increased dramatically due to the enhanced carrier space confinement, achieving a maximum PLQY of 92%, which was the state-of-the-art value among all the previous reported $MAPbBr_3$ films [78]. Based on the high-quality perovskite QW arrays with an average diameter of 6.4 nm and a length of about 200 nm, researchers achieved high-performance rigid PeLEDs on Si/SiO_2 substrates, with copper phthalocyanine (CuPc) as the hole injection and electron blocking layers [79] and indium zinc oxide (IZO) as the top electrode, respectively. As a consequence, the maximum current efficiency of the PeLEDs was 22.7 cd A^{-1} with a maximal EQE of 7.3% (Fig. 5f), which was a 90-fold improvement over those similar devices previously reported [80]. The highest brightness was up to 31,667 cd m^{-2}. These excellent properties were improved so much thanks to the high quality of polycrystalline $MAPbBr_3$ QW arrays and the enhanced radiative recombination due to the strong spatial confinement [77]. In addition, they demonstrated highly efficient flexible PeLEDs on Corning Willow glass with an emission area of 7 cm^2 with high

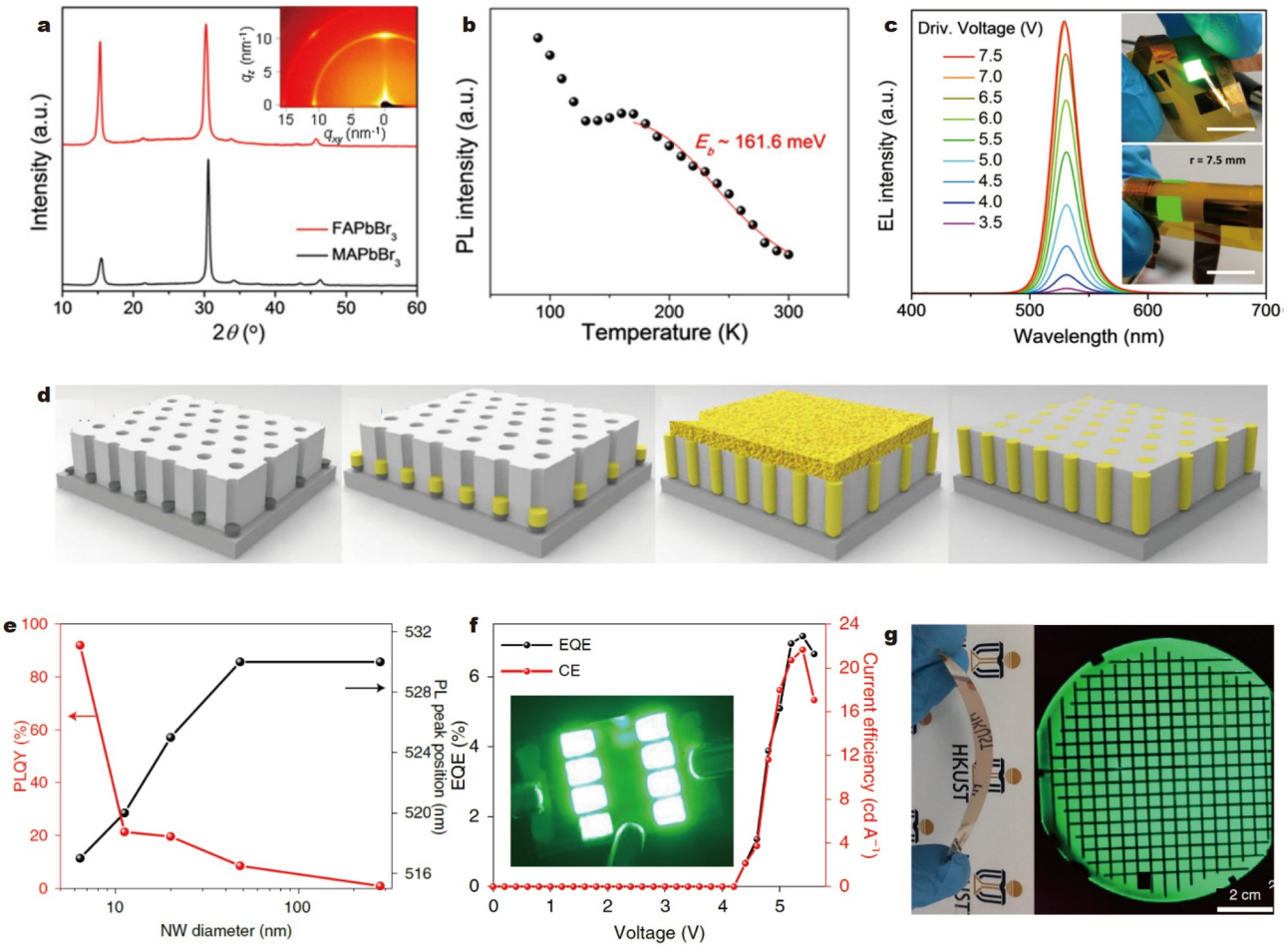

Figure 5 (a) The XRD patterns of the 2D perovskites ($FAPbBr_3$ and $MAPbBr_3$) films (inset: the GIWAXS image for the complex of 2D perovskites and PMMA). (b) The PL intensity of 2D perovskites and PMMA as a function of temperature, with the exciton binding energy of 161.6 meV in the cubic phase. (c) The EL spectra of the flexible PeLEDs with the driving voltage increasing from 3.5 to 7.5 V (inset: photographs of green flexible PeLEDs working at different bending radii). Reprinted with permission from Ref. [73]. Copyright 2017, American Chemical Society. (d) Schematic illustration of different growth stages of the CSVR method. (e) The PLQY values and PL peak positions of the perovskite QWs arrays with different diameters ranging from the quantum regime (6.4 nm) to the bulk regime (280.0 nm). (f) The EQE and current efficiency curves of the optimal rigid PeLEDs. Inset: photograph of the optimal PeLEDs. The size of every single emitting area is 2.0 mm × 2.8 mm). (g) Left image: an optical photograph of the flexible PeLEDs; right image: a photograph of a four-inch wafer-scale green PeLED with current distribution gridlines, demonstrating the flexibility and scalability, respectively. Reprinted with permission from Ref. [77]. Copyright 2022, Springer Nature.

flexibility and brightness, as shown in the left image of Fig. 5g. Furthermore, to test the adaptability and scalability of the innovative growth method including the PAM fabrication and CSVR process, large-area PeLEDs with four-inch wafer size were prepared for the first time. The right image in Fig. 5g shows the photograph of the wafer-scale PeLEDs with current distribution grid lines. Intriguingly, benefiting from the conformal nature of the proposed techniques, they achieved non-parallel 3D spherical PeLEDs by growing perovskite QWs on an Al sphere with $CsPbBr_3$ instead of $MAPbBr_3$ as the emissive layer. This unique planar device adopted a structure of $Al/Al_2O_3/CsPbBr_3$ QWs/NiO_x/IZO. Importantly, this spherical PeLED device exhibited excellent performance with a maximal EQE of 8.76% and a spatially uniform brightness of 1300 cd m^{-2}, providing a promising fabrication technique for the preparation of high-quality perovskite films and unconventional lighting applications in the future.

In addition to typical 3D/2D/quasi-2D MHPs, perovskite QDs are also considered as efficient emitting materials suitable for high-quality lighting and display applications due to their excellent optoelectronic properties, such as high PLQYs up to 100%, tunable emission wavelengths and narrow FWHM [81–85]. Moreover, the synthesis of perovskite QDs can be performed in solution, thus enabling rapid, mass production and compatibility with flexible devices [86–88]. As a result, perovskite QDs have also attracted substantial research interest in the field of flexible devices like SCs, detectors, and LEDs [89–91]. In recent years, perovskite QDs-based LEDs (QLEDs) have developed rapidly, achieving efficient green, red, and blue PeLEDs with the record EQEs of 22%, 21.3%, and 13.8%, respectively [92–94]. Li *et al.* [86] demonstrated stretchable PeLEDs with organometal-halide perovskite QDs as the emissive layer. Fig. 6a shows the transmission electron microscopy (TEM) image of the colloidal $MAPbBr_3$ QDs with an average diameter of 7 nm, which were synthesized by the emulsion method that they reported previously [95]. Ultra-thin QDs-based PeLEDs with the structure of VHB/PI/AgNWs/PEDOT:PSS/TAPC:PVK/perovskite QDs/TPBi/CsF/Al were prepared employing a com-

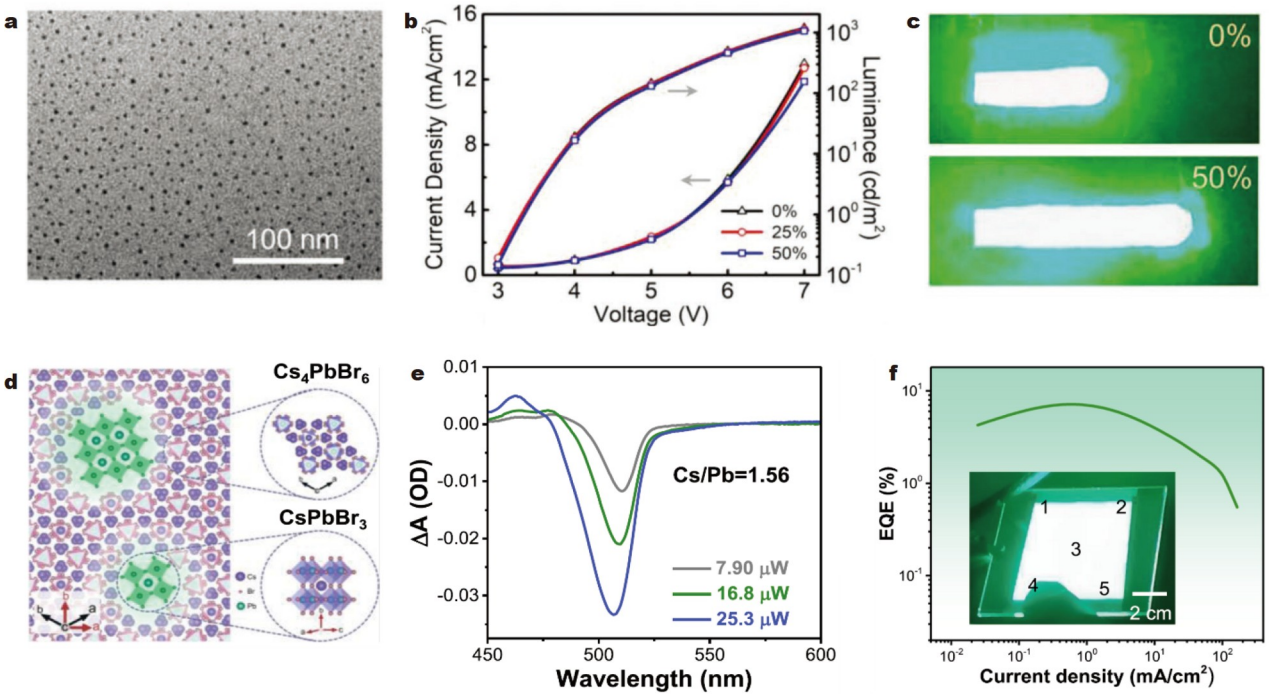

Figure 6 (a) TEM image of $MAPbBr_3$ QDs. (b) The current density and luminance curves as a function of voltage at various strains. (c) Photographs of the stretchable PeLEDs with strains of 0% and 50%. Reprinted with permission from Ref. [86]. Copyright 2019, Wiley-VCH. (d) The schematic illustration of the crystal model of $CsPbBr_3$ embedded in Cs_4PbBr_6. (e) The transient absorption spectra of $Cs_4PbBr_6/CsPbBr_3$ film with the ratio of Cs and Pb of 1.56. (f) The EQE curve as a function of the current density of the optimal large-area PeLEDs (inset: the optical photograph of the large-area PeLED with an area of 40.2 cm^2). Reprinted with permission from Ref. [97]. Copyright 2021, Springer Nature.

plex composed of AgNW network and 1–2 μm thick PI film as the ultra-flexible and highly conductive electrode. Fig. 6b shows the curves of current density and luminance with voltage (*J-V-L*) at different strains. It can be clearly seen that the current density and luminance maintained good operation stability when the device was stretched with strains ranging from 0% to 50%. More importantly, the optimal device showed excellent stretching performance and mechanical robustness. Fig. 6c displays the working photographs of the stretchable PeLEDs with different strains at a biased voltage of 7 V. The device exhibited highly uniform and bright emission with the strains ranging from 0% to 50%. Li *et al.* [96] proposed a simple one-step synthesis method of $CsPbBr_3$ QDs and ethylene vinyl acetate copolymer (EVA) films with high luminance, great stability, and flexibility. Based on this facile method, they demonstrated flexible white PeLEDs with the unique structure of INGnN chip/$CsPbBr_3$ QDs/EVA/$(Sr,Ca)AlSiN_3:Eu^{2+}$. The devices were highly flexible and stable, and the luminous intensity was almost constant even after 1000 bending cycles.

In addition to the direct synthesis of low-dimensional MHPs with only one single crystal structure component, the concept of core-shell structures in typical semiconductor NC systems such as CdSe/CdS and InAs/ZnSe can also be achieved by doping different structures of perovskites [98–100]. In 2017, Quan *et al.* [101] firstly synthesized a $CsPbBr_3/Cs_4PbBr_6$ core-shell structure by carefully controlling the stoichiometric ratio of CsBr and $PbBr_2$ in precursor solutions, in which $CsPbBr_3$ NCs were embedded in Cs_4PbBr_6 host matrix, achieving a high PLQY up to 90%. Xu *et al.* [99] further investigated the kinetics of the $CsPbBr_3/Cs_4PbBr_6$ system. In order to avoid the possible abscission of CsBr and control the components more accurately, Tan *et al.* [100] adopted the vacuum-evaporated method instead of the solution process to prepare perovskite films. Noticeably, they increased the content of Br^- by adding NaBr and LiBr, which partially converted $CsPbBr_3$ to $CsPb_2Br_5$ instead of Cs_4PbBr_6, resulting in a better stability against moisture and heat. In addition, Du *et al.* [97] reported the $Cs_4PbBr_6/CsPbBr_3$ core-shell structure by the vacuum thermal co-evaporation technique. By precisely controlling the evaporation rates of CsBr and $PbBr_2$, Cs-Pb-Br perovskite films with different Cs/Pb ratios could be prepared. Thanks to the incorporation of 0D Cs_4PbBr_6 into 3D $CsPbBr_3$ perovskites, the connectivity of $[PbBr_6]^{4-}$ octahedra was partially broken, leading to stronger spatial confinement. Fig. 6d shows the crystal model of the $Cs_4PbBr_6/CsPbBr_3$ core-shell structure with $CsPbBr_3$ embedded in the Cs_4PbBr_6 matrix. And the $CsBr/PbBr_2$ molar ratios determined the strength of spatial confinement [100]. Fig. 6e shows the transient absorption spectra of the perovskite films at a stoichiometric ratio of 1.56 of Cs to Pb. According to the fitting results from the spectra, the bi-molecular recombination constant k_2 of $Cs_4PbBr_6/CsPbBr_3$ films with Cs/Pb = 1.56 (9.34×10^{-10} cm^3 s^{-1}) was almost eight times higher than that of Cs/Pb = 1.24 (1.47×10^{-10} cm^3 s^{-1}). From the following formula, it is clear that the larger k_2 is, the higher the radiative efficiency η is,

$$\eta = \frac{k_2 n^2}{k_1 n + k_2 n^2 + k_3 n^3}, \quad (3)$$

where k_1 is the mono-molecular recombination constant, k_2 is the bi-molecular recombination constant, k_3 is the tri-molecular recombination constant, and n is the carrier density [2,102]. Therefore, the perovskite films with a higher Cs_4PbBr_6 content exhibited a higher radiative recombination rate due to stronger

spatial confinement. Furthermore, thanks to the good homogeneity and reliability of the vacuum thermal evaporation technique, they achieved efficient and large-scale rigid PeLEDs with an area of 90 cm^2 and flexible PeLEDs (300 mm^2) for the first time [103–105]. The inset in Fig. 6f shows a photograph of the large-area rigid PeLEDs. Most importantly, the fabricated large-scale PeLEDs exhibited excellent performance with the highest EQE up to 7.1% among all the reported devices using the thermal-evaporation system (Fig. 6f).

Mechanical properties

Since flexible PeLEDs should undergo stress tests to examine their flexibility, the great mechanical properties of perovskite films appear to be particularly important for flexible PeLEDs. Therefore, improving the mechanical properties of the perovskite emitting layers is essential to boost the performance of flexible PeLEDs. Lee *et al.* [106] investigated the flexibility of flexible PeLEDs in terms of tensile properties of the perovskite emissive layer. They fabricated flexible translucent PeLEDs with the device structure of PET/highly conductive mixture (PDZ)/$MAPbBr_3$/conjugated polyelectrolyte (SPW-111)/poly[(9,9-bis-(3′-(*N*,*N*-dimethylamino)propyl)-2,7-fluorene)-*alt*-2,7-(9,9-dioctylfluornene)] (PFN)/AgNW, as shown in Fig. 7a. To enhance the device efficiency, they utilized a conjugated polyelectrolyte (CPE) PFN as an interfacial layer between the ETL (SPW-111) and AgNW electrodes to reduce the electron injection potential barrier. The limits of mechanical robustness of the flexible PeLEDs were evaluated by measuring the brightness variation of the flexible PeLEDs at different bending radii (r_b). Fig. 7b shows the photograph of the flexible PeLEDs under the cyclic bending

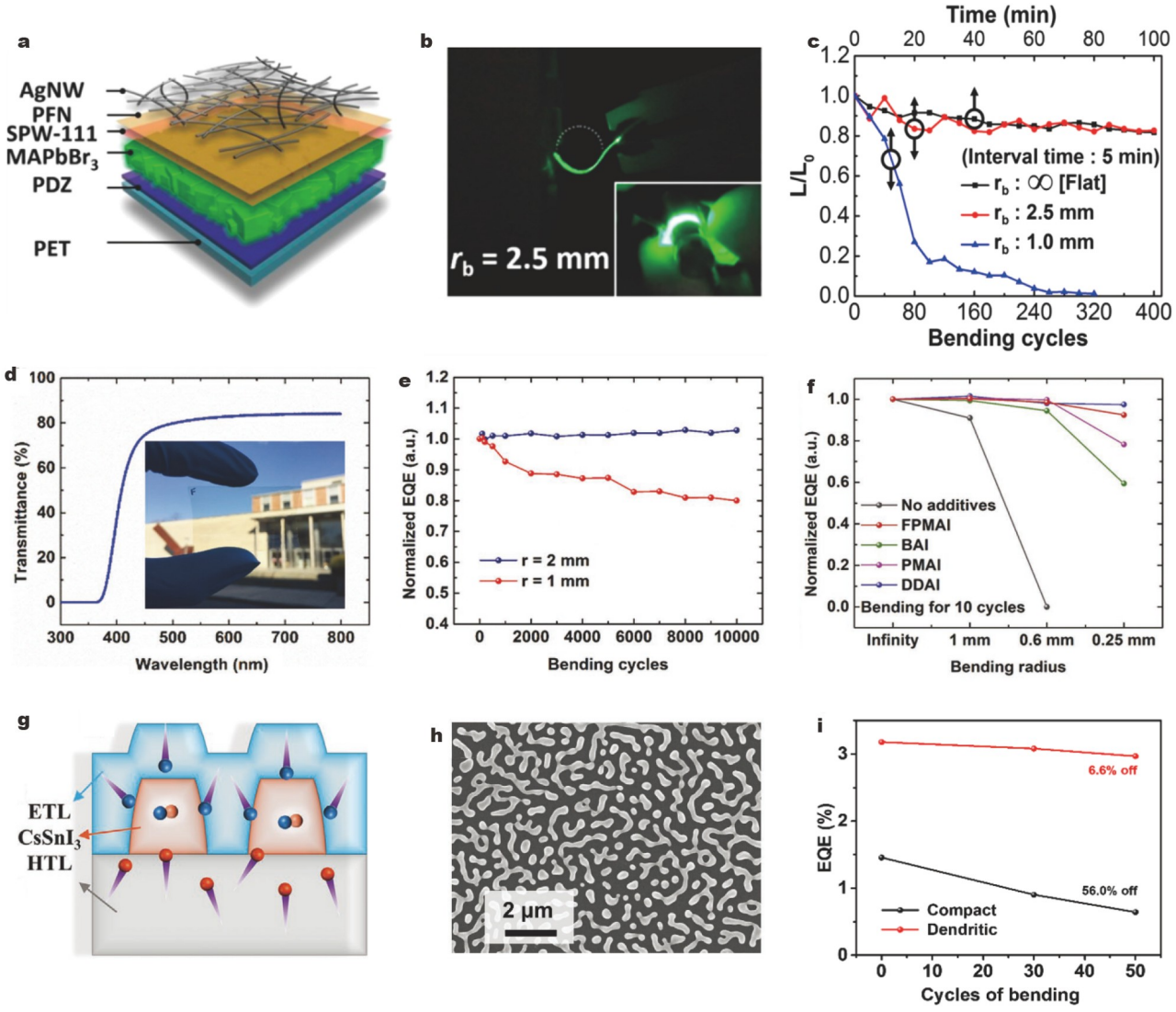

Figure 7 (a) Structural representation diagram of the flexible PeLEDs. (b) Photographs of the flexible PeLEDs under cyclic bending test with the bending radius of 2.5 mm. (c) Luminance changes of the flexible devices after different bending cycles with different bending radii. Reprinted with permission from Ref. [106]. Copyright 2019, American Chemical Society. (d) The transmittance spectrum of the flexible AgNW substrate (inset: the photograph of a flexible and transparent AgNW substrate). (e) Normalized EQE curves of the flexible PeLEDs after different bending cycles with the bending radii of 1 and 2 mm. (f) Normalized EQE curves of flexible PeLEDs with/without various additives after ten bending cycles with different bending radii. Reprinted with permission from Ref. [76]. Copyright 2018, Wiley-VCH. (g) Schematic illustration of the transport and recombination process of charge carriers in the dendritic $CsSnI_3$ films. (h) SEM image of the dendritic $CsSnI_3$ films after 2000 cycles of bending. (i) The EQE evolution curves of the compact and dendritic flexible PeLEDs after various bending cycles. Reprinted with permission from Ref. [108]. Copyright 2021, Wiley-VCH.

test with r_b = 2.5 mm. The results are shown in Fig. 7c. The luminance of the flexible PeLEDs with a bending radius of 2.5 mm and infinity was maintained at about 80% of the initial luminance. In contrast, when the bending radius was 1.0 mm, the luminance completely decreased after 320 bends, which could be ascribed to the mechanical failures (i.e., cracks and interfacial delamination). Moreover, the elastic modulus (28.15 (± 2.94) GPa) and yield strength (506 (± 58) MPa) of the $MAPbBr_3$ perovskite films were tested by the hole-nanoindentation test. In addition, they performed the same mechanical tests, including cyclic bending tests and hole-nanoindentation tests to PDZ and SPW-111. Finally, they found that the weakest material in their flexible PeLEDs was $MAPbBr_3$ perovskites [106]. The findings in these systematic studies provided a comprehensive guide for the further development of flexible PeLEDs. Zhao *et al.* [76] demonstrated that appropriate bulky organo-ammonium halide additives had a positive effect on the optoelectronic and mechanical properties of flexible PeLEDs. By adding five organo-ammonium halide additives with different alkyl chain lengths to $MAPbI_3$ perovskite precursors and measuring the PLQY values and cohesion energy (G_c) (reflecting the resistance and crack propagation of materials) of perovskite films [107], a balance between the optoelectronic and mechanical properties was found, which was further proved by quantum chemical calculations. This trade-off could be overcome by introducing electron-withdraw groups (e.g., fluorination) in the additives and thus enhancing the polarity. Furthermore, flexible PeLEDs with a AgNWs/PEDOT:PSS/poly-TPD/perovskite/TPBi/LiF/Al structure were achieved. As shown in Fig. 7d, the flexible AgNW substrates showed excellent mechanical properties with a transmittance of about 80%. The inset in Fig. 7d shows an optical photograph of the translucent flexible AgNW substrate. The flexibility of the flexible PeLEDs was examined by cyclic bending tests. There was no significant degradation of EQE after 10,000 bending cycles for the flexible PeLEDs with a bending radius of 2 mm, and almost 80% of the initial EQE (13%) remained unchanged after 10,000 bending cycles for a bending radius of 1 mm (Fig. 7e). Moreover, the mechanical robustness of the perovskite films was significantly enhanced with the incorporation of different additives, compared with the perovskite films without any additives, and there was no significant EQE degradation even when the flexible devices were bent at a radius of 0.25 mm (Fig. 7f).

Recently, Lu *et al.* [108] reported efficient flexible NIR PeLEDs using $CsSnI_3$ perovskites instead of $CsPbBr_3$ perovskites as the emitting layer. The $CsSnI_3$ had a unique dendritic structure that allowed only one side to contact with the HTL and the other sides to contact with the ETL, as shown in Fig. 7g. On the one hand, this special structure could enhance the electron injection; on the other hand, it could limit the undirected diffusion of holes and improve the radiative recombination. Based on the unique dendritic $CsSnI_3$ perovskites, the researchers demonstrated rigid NIR PeLEDs with the EL peak at 932 nm and achieved the recorded EQE of 5.4% among all the lead-free PeLEDs. Furthermore, to explore the feasibility of the unique dendritic $CsSnI_3$ perovskites for flexible PeLEDs, researchers fabricated flexible NIR PeLEDs on PEN substrates. The dense and dendritic $CsSnI_3$ films were subjected to 2000 bending cycles to test their mechanical stability. Unlike the appearance of obvious cracks in compact $CsSnI_3$ films, the dendritic $CsSnI_3$ films did not show any visible cracks, as shown in Fig. 7h. Therefore, the dendritic $CsSnI_3$ perovskite films had better flexibility. To test the operating stability of the corresponding flexible PeLEDs, the EQE changes of both the compact and dendritic flexible PeLEDs were measured under different bending cycles. As shown in Fig. 7i, after 50 bending cycles, the EQE of the compact PeLEDs decreased to 56% of the initial EQE (1.5%), while the EQE of the dendritic PeLEDs only lost 6.6%, exhibiting excellent mechanical properties. Inspired by these interesting results, perovskites with specific dendritic structures or other unique structures may be candidates for efficient and stable flexible PeLEDs.

Light extraction

As mentioned in the INTRODUCTION section, the EQE could be calculated with the formula EQE = IQE × η_{oc}, where η_{oc} is the light outcoupling efficiency [65,109]. However, not all the generated photons can be emitted into free space, as they might be captured by emitting materials, electrodes, and substrates [13,78]. Since the IQE which could be estimated from PLQYs has already approached unity, improving the light outcoupling efficiency has become the most critical factor to further improving the device performance [78,110,111]. In general, by introducing nanostructures in PeLEDs, it is possible to couple out the waveguide modes and thus improve the light outcoupling efficiency [110]. Many reports have demonstrated numerous efficient light-extraction technologies by introducing micro-photonic structures in the PeLEDs and OLEDs devices. For instance, nanophotonic substrates [112], micro-lens arrays [113], diffraction gratings [114], and contrast nanoarrays [115] with high index have been employed at appropriate device interfaces to greatly improve the outcoupling efficiency of conventional organic and inorganic LEDs.

Shen *et al.* [116] presented highly efficient green PeLEDs with outcoupling enhancement *via* nanoimprinted moth-eye nanostructures together with hemispherical lenses. The results showed a maximum EQE of 28.2% and a current efficiency of 88.7 cd A^{-1}, which were the highest values up to date. Furthermore, based on their inspiring findings, they combined rational interface engineering with quasi-random patterned flexible substrates [20] to prepare highly efficient flexible PeLEDs. Fig. 8a illustrates the schematic fabrication process of the flexible PeLEDs. They used plastic PET substrates instead of rigid ITO-glass substrates to fabricate flexible devices. The flexible transparent electrode consisted of AgNWs and patterned ZnO. The patterned structure was proved to be able to enhance the outcoupling efficiency [116]. The final flexible PeLEDs devices had an architecture of PET/AgNWs/ZnO/PEDOT:PSS/$CsPbBr_3$/TPBi/LiF/Al (Fig. 8a). Moreover, perovskite crystallization with defect passivation and interface stimulation was implemented by incorporating an amino additive ethanolamine (ETA) into the $CsPbBr_3$ precursors to modulate the underlying interlayer and suppress the non-radiative recombination. Fig. 8b shows the angular dependence of EL intensities and the EL spectrum of the flexible PeLEDs with planar and patterned structures. When the viewing angle varied from 0° to 80°, there was no visible change in the EL intensity, approaching the perfect Lambertian pattern. Meanwhile, the flexible PeLEDs showed high reproducibility with a maximum EQE of 24.5% for the flexible PeLEDs with patterned electrodes, which was significantly improved compared with the flexible PeLEDs with flat flexible transparent electrodes (17.1%) (Fig. 8c). The mechanical flexibility of the

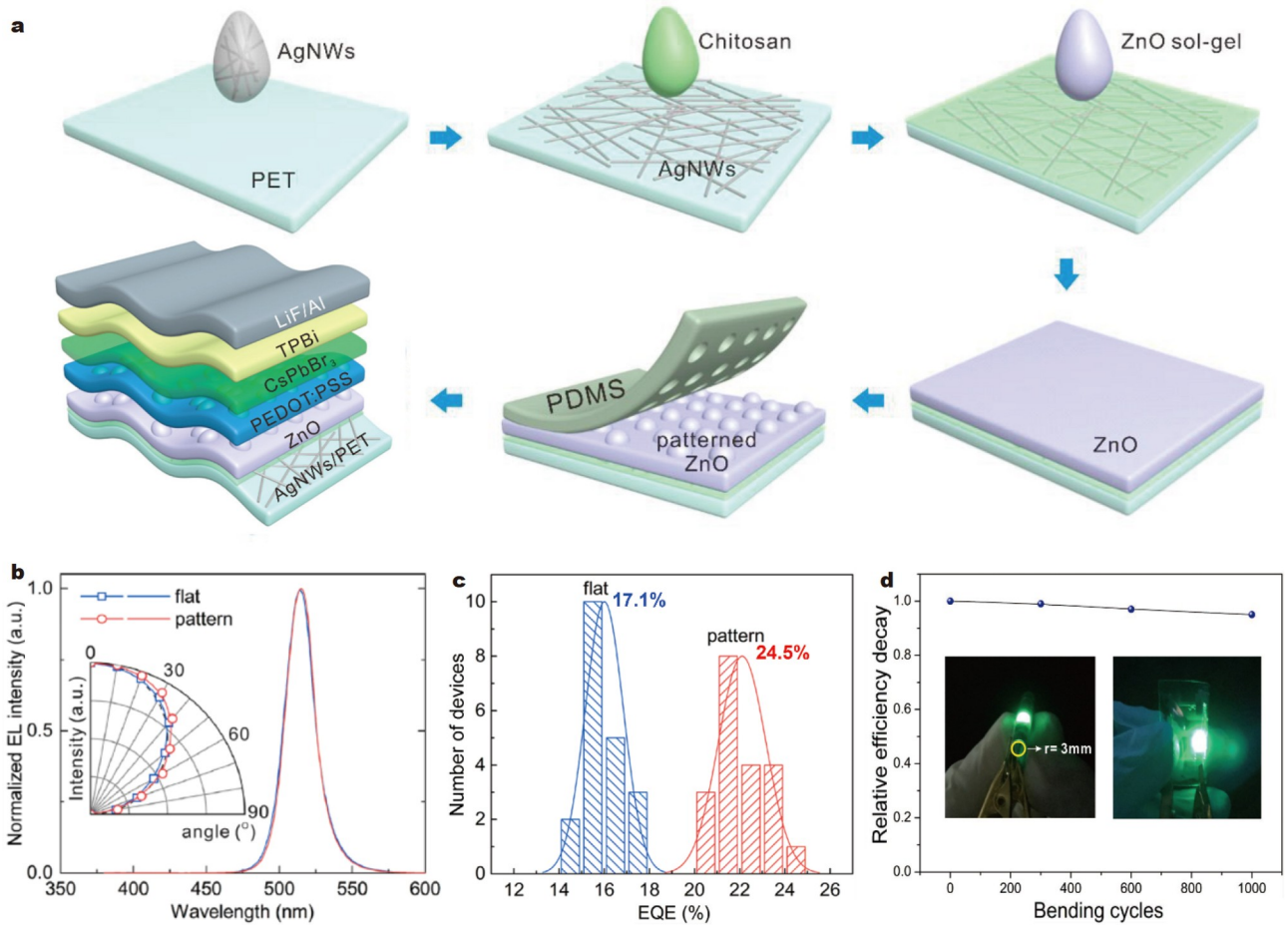

Figure 8 (a) Schematic illustration of the fabrication process of the flexible transparent electrode, including the device structure of flexible PeLEDs. (b) Normalized EL spectra of the flexible PeLEDs with flat or pattern structures (inset: the angular-dependence curves of the EL intensities of the flexible PeLEDs with two different structures). (c) The maximum EQE histograms of the flexible PeLEDs with flat and patterned flexible transparent electrodes, with the maximum EQEs of 17.1% and 24.5%, respectively. (d) The relative efficiency changing curve *versus* bending cycles (inset: photographs of the flexible PeLEDs under bending test with a radius of curvature of 3 mm). Reprinted with permission from Ref. [20]. Copyright 2020, American Chemical Society.

ETA-modified flexible PeLEDs was examined by the cyclic bending tests. As shown in Fig. 8d, the relative efficiency remained almost 90% of the initial efficiency after bending for 1000 times with a bending radius of 3 mm, exhibiting excellent mechanical stability.

Charge transporting layers

Hole transporting layer

The ideal CTLs including HTLs and ETLs, with multiple functions of balancing charge injection and blocking opposite charges, have a great impact on the performance of PeLEDs [117]. Among all the HTL materials, PEDOT:PSS and its derivatives have been intensively investigated and were considered as a group of effective HTL materials due to their solution processibility, high conductivity, and optical transmittance [118–120]. However, it has been reported that PEDOT:PSS could jeopardize the device performance due to its high hole injection barrier as well as acidic and hygroscopic nature [121,122]. To reduce the huge energy barrier to the emitting layer, Kim *et al.* [123] proposed a facile strategy to increase the work function of PEDOT:PSS. By mixing pristine PEDOT:PSS aqueous solution with two other different solutions, isopropyl alcohol (IPA) and poly(sodium 4-styrene sulfonate) (PSS-Na), they increased the work function of HTLs from the original 5.18 to 5.46 eV. Based on this, they fabricated flexible PeLEDs and greatly improved the device performance, and realized a maximum current efficiency of 25.13 cd A^{-1} and the best EQE of 5.91%. Similarly, Lee *et al.* [124] successfully reduced the hole injection barrier of PEDOT:PSS through the incorporation of a non-conductive fluor-surfactant. With the assistance of introducing Zonyl FS-300 (Zonyl) into the PEDOT:PSS layer, the work function was significantly increased to 5.45 eV and the luminance quenching at the interface between the PEDOT:PSS and perovskite emitting layer was also reduced (Fig. 9a). They further demonstrated flexible PeLEDs with various electrodes, including PEDOT:PSS, AgNWs, composites, and PEN/ITO electrodes. Fig. 9b shows the current efficiency *versus* voltage curves of the flexible PeLEDs with different electrodes. The flexible PeLEDs prepared with composite electrodes exhibited the best performance, with a maximum current efficiency of 17.90 cd A^{-1}. In addition, they performed continuous bending tests to check the mechanical flexibility of the flexible devices. The flexible PeLEDs maintained 94% of the initial brightness (127.2 cd m^{-2}) after 1000 bending cycles at a radius of 2.5 mm. And the devices were able to operate normally at the extreme

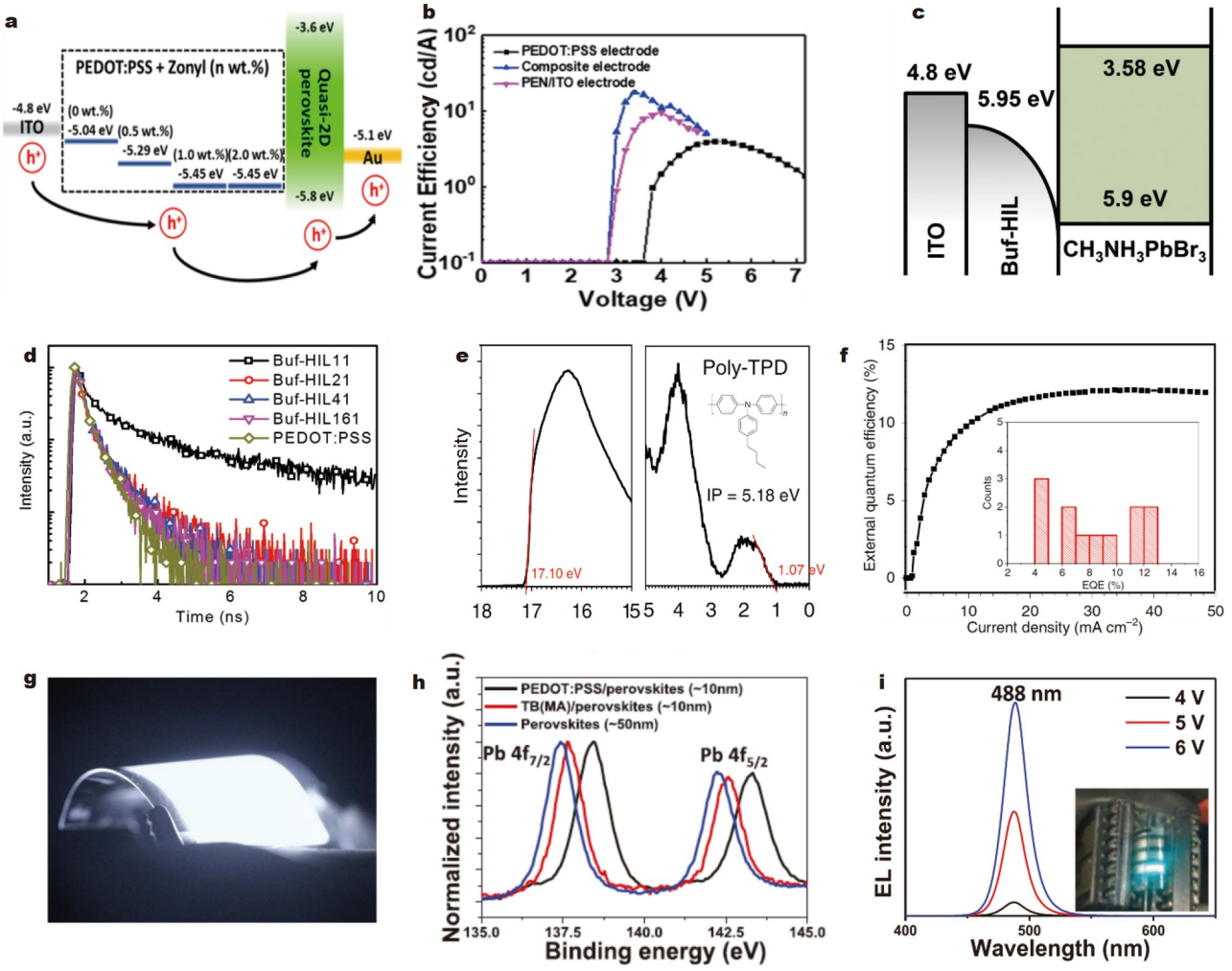

Figure 9 (a) Schematic illustration of the hole transportation process through HTLs composed of PEDOT:PSS and various concentrations of Zonyl. (b) The current efficiency curves of the flexible PeLEDs with different electrodes. Reprinted with permission from Ref. [124]. Copyright 2019, American Chemical Society. (c) Energy-level diagram with a gradual changing of Bul-HTL work function. (d) TR-PL curves of perovskite films with various HTLs. Reprinted with permission from Ref. [16]. Copyright 2014, Wiley-VCH. (e) The ultraviolet photoelectron spectroscopy (UPS) spectra of poly-TPD (inset: the chemical structure of poly-TPD). (f) The EQE *versus* the current density curve of the flexible PeLEDs with a large area of 900 mm^2 (inset: the maximum EQE histogram of 12 flexible devices). (g) NIR photograph of the flexible large-area PeLEDs. Reprinted with permission from Ref. [19]. Copyright 2019, Springer Nature. (h) XPS spectra of perovskite films with different HTLs. (i) EL emission spectra of the flexible sky-blue PeLEDs (inset: photograph of a flexible PeLED in a bent state). Reprinted with permission from Ref. [117]. Copyright 2021, Wiley-VCH.

bending radius of 1.5 mm, showing excellent mechanical stability.

In addition to PEDOT:PSS, researchers have developed other novel materials as efficient HTLs. Kim *et al.* [16] demonstrated a self-organized buffer HTL (Buf-HTL) consisting of PEDOT:PSS and PFI. Due to the self-organization of PFI, the work function of Buf-HTL gradually changed from 5.20 eV on the lower surface to 5.95 eV on the upper surface, as shown in the schematic energy level diagram in Fig. 9c. This gradual change in the work function could reduce the hole injection barrier and limit the exciton quenching, thus improving the hole injection and device performance. Fig. 9d shows the time-resolved PL (TR-PL) spectra of the perovskite films with various Buf-HTLs. The sample with the addition of Buf-HTL11 (the weight ratio of PEDOT:PSS and PFI is 1:1) exhibited the longest lifetime (4.7 ns with about 10-fold enhancement), which may be related to the suppression of exciton dissociation and enhanced hole transfer [16]. The performance of the Buf-HTL-based PeLED devices was more than 300 times better than that of the PeLEDs with conventional PEDOT:PSS, with a maximum brightness of 417 cd m^{-2} and a maximal EQE of 0.125%. More importantly, they prepared the first flexible PeLEDs with the device structure of PET/ITO/Buf-HTL/$CH_3NH_3PbBr_3$/TPBi/LiF/Al, showing the potential of organic/inorganic hybrid perovskites in flexible optoelectronic devices. Zhao *et al.* [19] pointed out that the springhead of suboptimal PeLEDs was located in the inferior hole injection. To overcome this problem, they utilized a novel hole-transporting material poly-TPD, which had a shallower ionization potential of 5.18 eV below the vacuum level (Fig. 9e). The shallower ionization potential of poly-TPD favored the hole transport, which could be ascribed to the Fermi-level pinning effect [125,126]. With this efficient HTL material, they successfully prepared one of the most representative rigid NIR PeLEDs with a maximum EQE of up to 20.2%. Furthermore,

they demonstrated efficient large-area flexible PeLEDs. Fig. 9f presents the EQE *versus* the current density curve and the inset shows the maximum EQE histograms of 12 flexible PeLED devices. The average EQE of the flexible devices was 8.2% and the highest value was 12.1%. Fig. 9g shows a photograph of the flexible NIR PeLEDs with an area of 900 mm^2.

In addition, Liu *et al.* [117] adopted a water-soluble CPE with thiophene units and MA^+ ions (TB (MA)) as the HTL and prepared highly efficient flexible sky-blue PeLEDs. Fig. 9h shows the X-ray photoelectron spectroscopy (XPS) spectra of the perovskite films with different HTLs. Compared with the main peaks corresponding to Pb $4f_{7/2}$ and Pb $4f_{5/2}$ of the pristine samples, the peak displacements of the perovskite films with TB (MA) as HTL were much smaller than those of the perovskite films with PEDOT:PSS as HTL, indicating lower halide vacancies, which could be attributed to the successful passivation of the uncoordinated halide defects. On the other hand, the hydrophilicity nature of TB (MA) could improve the surface quality of the perovskite films and make their morphology compact and uniform. Sky-blue flexible PeLEDs were prepared using TB (MA) as HTL, with the device structure of PEN-ITO/TB (MA)/perovskite/TPBi/LiF/Al. The optimal device exhibited the maximum EQE of 8.3% and brightness of 2967 cd m^{-2}. Fig. 9i shows a photograph of the flexible PeLEDs with the EL emission peak at 488 nm.

Electron transporting layer

Recently, the optimization of ETLs has attracted lots of attention to achieve high-performance PeLEDs. However, they have almost all focused exclusively on rigid PeLEDs, but little has been reported on flexible PeLEDs. Nevertheless, due to the great similarity between the rigid and flexible PeLEDs, newly developed materials for efficient ETLs or proven feasible strategies for optimizing ETLs in rigid PeLEDs have great potential to be employed in flexible PeLEDs. ZnO has been utilized as a suitable ETL material that facilitated the electron injection and blocked hole transport [127–129]. Qasim *et al.* [130] designed a new n-type ETL by the sol-gel method to dope calcium (Ca) into ZnO. With the assistance of the Ca dopant, the ZnO energy band structure produced cascade energy levels, which improved the electrical conductivity and carrier mobility of the Ca-doped ZnO ETLs. Employing this doped ETL material, researchers prepared red, yellow, and green PeLEDs, with maximum EQEs of 5.8%, 4.2%, and 6.2%, respectively, indicating good applicability of this novel ETL. Likewise, Tang *et al.* [131] incorporated cobalt (Co) into ZnO and synthesized Co-doped ZnO as ETL. Co dopant could passivate the oxygen vacancies and trap electrons, thus reducing the electron mobility and regulating the energy levels. Additionally, the incorporation of Co could improve the quality of perovskite films and suppress the exciton quenching. The results showed that the PeLEDs with Co-doped ZnO as ETL exhibited good performance with a maximum luminance of 1858 cd m^{-2}, an optimum EQE of 13.0%, and an enhancement rate of 70%. Besides, Lu *et al.* [132] reported a new type of ETL mixed with Ti_3C_2-MXene and ZnO NCs. On the one hand, the introduction of Ti_3C_2 could significantly reduce the electron mobility by two orders of magnitude and balance the carrier transport. On the other hand, the relatively smooth ETL could enable the uniform distribution of perovskite. As a result, the EQE of the final PeLED devices reached a maximal EQE of 17.4%. In addition, new ETL materials have been developed to improve the device performance. Based on the commonly used ETL, TPBi, Liu *et al.* [133] reported a new ETL termed as TPBi/tris(8-hydroxyquinoline) aluminum (Alq_3)/TPBi by introducing Alq_3 into TPBi. The addition of Alq_3 could not only balance the charge carrier transport but also enhance the charge space confinement. Ultimately, the performance of the PeLEDs using TPBi/Alq_3/TPBi as ETL was improved greatly. In addition, Cai *et al.* [134] demonstrated high-performance PeLEDs by rational tunning the chemical structure of ETLs, achieving high carrier mobility and effective passivation. Furthermore, Fang *et al.* [135] and Sun *et al.* [136] proposed specific dual ETL structures to boost the performance of PeLEDs, respectively. With the help of the unique double-layer electron-transporting structure, better charge carrier injection balance and exciton quenching suppression were achieved. Consequently, high-performance rigid PeLEDs with the highest EQEs of 21.63% and 10.7% were achieved, respectively.

Flexible electrodes

Metal-based flexible electrodes

Metals (e.g., Ag, gold (Au), aluminum (Al), and copper (Cu)) have been widely used as flexible electrodes in the field of flexible optoelectronic devices due to their high electrical conductivity, good mechanical flexibility, and robustness [13]. AgNWs are the most used flexible electrode materials. In general, AgNW electrodes could be prepared liberally *via* the solution method. Zhao *et al.* [88] prepared highly flexible PeLEDs with high mechanical stability using solution-prepared AgNWs-based polymer electrodes as flexible anodes and $MAPbBr_3$ QDs as the emitting layer, and there was no significant degradation in performance after 1000 bending cycles at a bending radius of 2.5 mm. To improve the stretchability and flexibility of AgNW electrodes, Lee *et al.* [137] reported a novel sequential multistep growth method (SMG) for the growth of long-length AgNWs. The length of AgNWs was successfully increased from 20 μm to more than 500 μm with advanced mechanical compliance and conductivity by continuous multiple-step synthesis.

Carbon-based flexible electrodes

Compared with metal-based electrodes, carbon-based electrodes such as CNTs and graphene have high transmittance, high carrier mobility, good mechanical flexibility, and solution processibility, making them potential candidates for flexible and transparent electrodes suitable for flexible optoelectronic devices [138–141]. Zhang *et al.* [142] demonstrated transparent and strong single-walled CNTs with gravimetric strength even higher than that of steel. Furthermore, these self-supporting CNTs have been shown to be used as transparent and highly elastomeric electrodes for flexible lighting devices. Bade *et al.* [49] prepared highly flexible PeLEDs with CNTs as the flexible transparent electrodes. It is worth mentioning that they reported a fabrication process based on a complete printing method. With fully-printed perovskites and AgNWs as the emitter and cathode, respectively, they obtained rigid green PeLEDs with a maximum luminance intensity of up to 21,014 cd m^{-2} and the highest EQE of 1.1%. In addition, flexible PeLEDs based on CNTs/polymer substrates exhibited excellent mechanical stability without observable degradation in device performance at a bending radius of curvature of 5 mm. Seo *et al.* [17] creatively demonstrated the feasibility of graphene as the anodes. they prepared

high-performance flexible PeLEDs without ITO layer by using four layers of graphene as the electrodes, a special self-organized buffer hole injection layer (Buf-HTL) as the HTL [16], and $MAPbBr_3$ perovskite as the emitting layer. In conventional ITO-based PeLEDs, the migration of indium (In) and tin (Sn) atoms at the interface between the perovskite emitting layer and HTL resulting in the exciton quenching could significantly damage the device performance. However, the use of graphene electrodes could eliminate this detrimental effect of ITO and greatly improve the PL intensity and lifetime. Fig. 10a shows the schematic illustration of the exciton quenching by In and Sn atoms in ITO-based PeLEDs and the enhanced luminescence in graphene-based PeLEDs. In addition, due to the excellent flexibility of graphene electrodes, the researchers fabricated flexible PeLEDs with the structure of PET/graphene/Buf-HTL/$MAPbBr_3$/TPBi/LiF/Al, as shown in the inset in Fig. 10b. The performance of the flexible graphene-based PeLEDs elevated markedly thanks to the reduction of luminescence quenching. Fig. 10b shows the current efficiency curve of the graphene-based flexible PeLEDs. The maximal current efficiency reached 16.1 cd A^{-1} and the highest brightness was 13,000 cd m^{-2}. Furthermore, the typical cyclic bending test was performed to verify the flexibility and mechanical robustness of the flexible devices. After 1200 cycles of bending at a bending radius of 7.5 mm and a strain of 1.34%, the current density retained about 81% of the initial value. Only when the device experienced extreme bending with a radius of curvature of 1.9 mm and a strain of 5.3%, did it fail, showing reliable flexibility and stability. Zhang *et al.* [143] also utilized graphene as the electrode for QD-based PeLEDs. In order to overcome the poor film uniformity resulting from hydrophobicity, they proposed a modified PEDOT:PSS consisting of DMSO and the surfactant triton X-100. Ultimately, the surface quality of the perovskite films and the wettability of graphene were greatly improved and showed a progressive EQE of 2.58%.

Polymer flexible electrodes

In addition to metal and carbon-based electrodes, polymers with high electrical conductivity and flexibility can also be used as electrodes, such as PEDOT:PSS, poly(3-hexylthiophene) (P3HT), polyacetylene, and their derivatives [145–147]. Wegner [148] summarized the synthesis, structures, and properties of these metal-like polymers. Jeong *et al.* [144] developed a novel universal polymer electrode with both anode and hole transport dual function, namely Anode-HTL (AnoHTL). This multifunctional AnoHTL involved a high-conductivity polymer PEDOT:PSS for conduction, a polar additive DMSO as the conductivity enhancer, and an acidic copolymer tetrafluoroethylene-perfluoro-3,6-dioxa-4-methyl-7-octenesulphonic (PFSA) as the work function regulator. Fig. 10c shows the schematic illustration of the AnoHTL electrode with two different functional components and the hole injection process from the AnoHTL anode to the adjacent semiconducting layer. Due to the low surface energy of PFSA, it tended to accumulate on the surface of the AnoHTL film. The upper part was mainly PFSA with higher tunable work function and lower conductivity

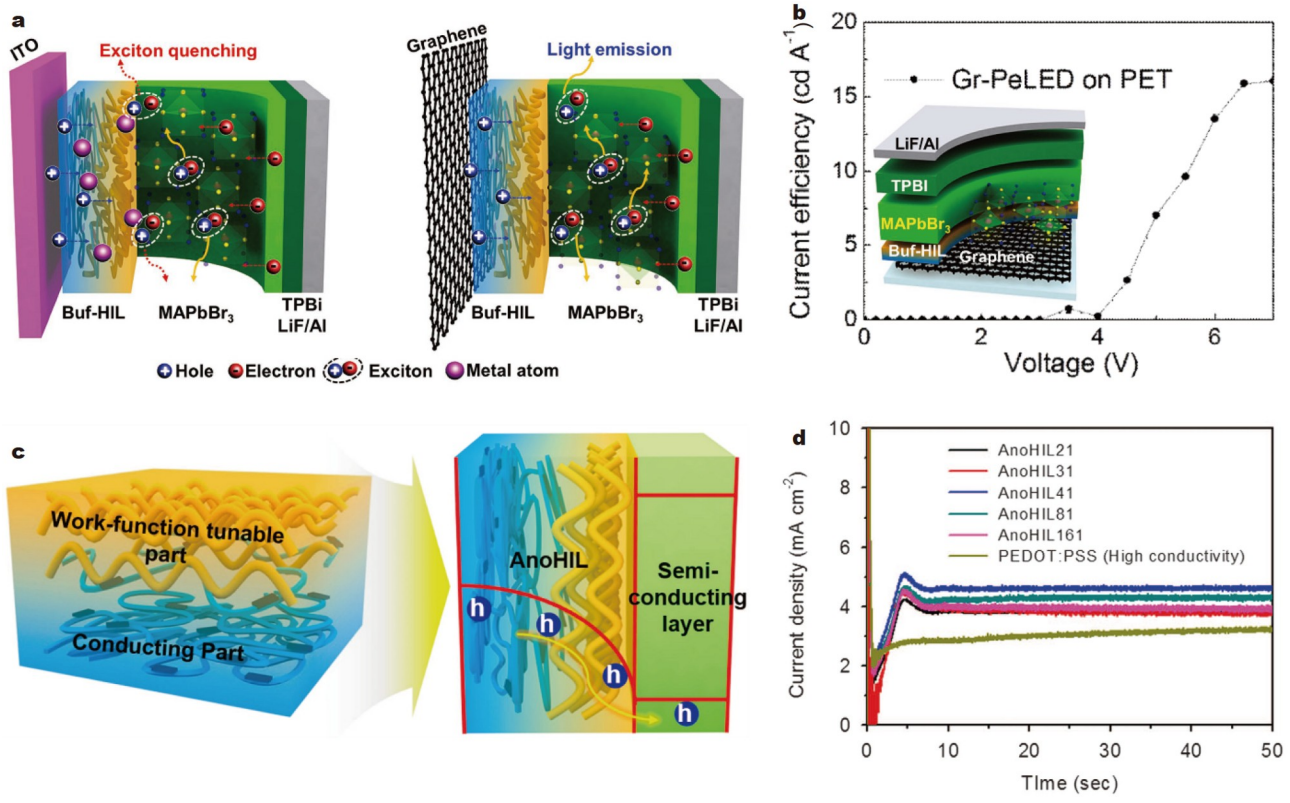

Figure 10 (a) Schematic illustration of the exciton quenching resulting from In and Sn atoms in ITO-based PeLEDs and circumvent of this process in graphene-based PeLEDs. (b) The current efficiency *versus* voltage curve of the flexible graphene-based PeLEDs (inset: structural representation of the flexible PeLEDs on PET flexible substrate). Reprinted with permission from Ref. [17]. Copyright 2017, Wiley-VCH. (c) Schematic illustration of the difunctional AnoHTL and the hole injection process from the AnoHTL into an overlaying semiconducting layer. (d) The DI-SCLC *versus* time curves of various polymeric anodes. Reprinted with permission from Ref. [144]. Copyright 2017, Springer Nature.

as the HTL, while the lower part was primarily PEDOT:PSS as the anode. In addition, the ohmic contact was formed at the interface between the semiconductor layer and AnoHTL, which could be demonstrated by measuring the dark injection space-charge limited current (DI-SCLC). The results were shown in Fig. 10d, where the peak DI-SCLC transient signal appeared only in the AnoHTL-based devices, indicating the presence of ohmic contact [149,150]. Based on this novel AnoHTL, researchers fabricated ITO-free flexible PeLEDs, with a simplified AnoHTL/$MAPbBr_3$/TPBi/LiF/Al device structure. The devices showed excellent performance, with an EQE of up to 8.66% and a maximum current efficiency of 42 cd A^{-1}.

Flexible substrates

The substrates suitable for flexible PeLEDs must have excellent flexibility, mechanical robustness, high light transmittance, and good stability. Currently, flexible transparent polymer substrates are the most commonly used flexible substrates, such as PET [16,56], PEN [55,117], PI [73,76], polyurethane (PU) [151], and other polymers [49,124,152]. Furthermore, Ag mesh could sometimes be embedded in the polymer substrates in order to enhance the optical and electrical properties of flexible transparent substrates [153]. Overall, it is worthwhile to put effort into developing new materials applicable for flexible and transparent substrates with better performance. Additionally, we summarize the recent reports including the device structures and key performance parameters in the field of flexible PeLEDs, as shown in Table 1.

CHALLENGES OF FLEXIBLE PeLEDs

In the previous section, most breakthroughs in flexible PeLEDs have been summarized. However, compared with relatively mature flexible OLEDs, flexible PeLEDs with the potential to be integrated into flexible, portable, and wearable platforms are still in their infancy. There are still several hurdles to the pragmatic application, which require more research attention and efforts in physical and mechanism understanding, materials innovation, new device structures, and new fabrication techniques [158].

Stability

Currently, one of the most focused issues in the field of perovskite optoelectronics is how to improve the stability of perovskite films under the joint influence of air, moisture, light, and heat. Sun and co-workers [159] comprehensively reviewed the recent progress in PeLEDs with enhanced spectral and operational stability. Besides perovskite films and device structure engineering, they pointed out that the stability could be improved by suppressing the ion migration and the Joule heating, and increasing the light outcoupling efficiency. In addition to the device stability, attention should also be paid to the thermal stability. Zhang *et al.* [160] revealed that defects could promote stronger exciton-phonon coupling and thus induce the emission thermal quenching and decrease the luminescence efficiency of quasi-2D PeLEDs. Moreover, proper macro/microencapsulation is considered to be the most efficient way to achieve flexible PeLEDs with long-term stability [161]. Especially for the flexible PeLEDs, the mechanical properties of perovskite emitting materials should be emphasized. Chen *et al.* [162] investigated the variation of the perovskite films under a series of bending tests and the full dimensional release of the grain boundary stresses in flexible perovskite indoor photovoltaics. The effective strategy was instructive for improving the operational stability and the performance release of flexible PeLEDs.

Mechanical robustness

The mechanical robustness problem mainly originates from electrodes, both metallic and others. As mentioned previously, many reports have demonstrated potentially alternative flexible electrodes, such as AgNWs [76,88,106,154], graphene [17,143], and other polymers [49,73,151,152]. Although these electrodes exhibit better mechanical stability than the conventional metal electrodes (Au, Ag, Cu, Al, etc.), flexible PeLEDs based on these electrodes suffer from low efficiencies. Due to the proper work function, better mechanical robustness, and environmental stability, graphene-based electrodes are considered as appropriate candidates for flexible PeLEDs. However, the poor electrical conductivity of these materials limits their further applications. Therefore, a systematic and in-depth study and development of graphene and its derivatives as well as other novel materials suitable for flexible devices is essential.

Flexible blue and red PeLEDs

Currently, almost all the flexible PeLEDs with considerable EQEs are monochromatic green light emitting [18,20,97,144]. Nevertheless, balanced and efficient green, red, and blue light emissions are essential for full-color displays and colorful illumination [163]. The state-of-the-art EQEs of green and red rigid PeLEDs have exceeded 20% [6,11,93,164], while that of blue PeLEDs on rigid substrates is only 13.8% [94]. The EQEs of flexible PeLEDs are even smaller. Hence, how to realize efficient flexible PeLEDs based on the existing research results and how to improve the performance of blue PeLEDs both on rigid and flexible substrates should be resolved to further promote the development of flexible PeLEDs and next-generation displays.

Toxicity

Since flexible PeLEDs could be integrated into portable and wearable platforms, showing great potential in wearable electronics and biomedical devices, unacceptable toxicity for consumers must be taken into account [165]. The main source of toxicity is the elemental lead in MHPs. Through completely or partially replacing the Pb element in perovskites, lead-free or less-lead PeLEDs can be obtained, thus reducing the toxicity. In general, the possible alternative elements for the B-site Pb element include Sn [166,167], strontium (Sr) [94,168,169], zinc (Zn) [170,171], manganese (Mn) [172,173], and others [170,174–177]. However, the current PeLEDs based on these substitutional components suffer from poor stability and low efficiency. Therefore, more efforts deserve to be taken to further develop non-toxic and environment-friendly flexible PeLEDs.

Large-area fabrication

In order to meet the growing consumer demand, large-area displays and illumination based on MHPs show an urgent need for development. However, as the device area grows, the series resistance and electrical uniformity will increase dramatically, thus reducing the operational stability and efficiency of flexible PeLEDs [38,161]. Also, the quality of perovskite films will deteriorate with the proliferation of defects and pinholes as well as the reduction of film homogeneity [178]. In addition, the conventional spin-coating method is not suitable for preparing

Table 1 Summary of the performance of flexible PeLEDs recently reported

Device architecture	EL (nm)	EQE (%)	CE_{max} (cd A^{-1})	L_{max} (cd m^{-2})	Bending radius (mm)	Strain (%)	Ref.
PET/ITO/Buf-HTL/$MAPbBr_3$/TPBi/Al	543	0.125	0.557	417	105	–	[16]
Graphene/Buf-HTL/$MAPbBr_3$/TPBi/LiF/Al	542	3.8	18.0	13,000	7.5	–	[17]
PET/PEDOT:PSS/$CsPbBr_3$/TPBi/LiF/AgNWs	521	10.1	31	45,990	–	–	[18]
PET/ITO/ZnO/PEIE[a]/$FAPbBr_3$/poly-TPD/MoO_3/Al	799	12.1	–	–	–	–	[19]
AgNWs/PET/ZnO/PEDOT:PSS/$CsPbBr_3$/TPBi/LiF/Al	514	24.5	75	10,000	3	–	[20]
Polyacrylate/CNTs/PEO/perovskite/TPBi/AgNWs	545	0.14	0.6	360	~5	–	[49]
Substrate/ITO/HATCN[b]/TAPC[c]/$CsPbBr_3$/PO-T2T[d]/Liq/Al	520	3.26	10.3	17,550	–	–	[54]
PEN/PEDOT:PSS/$MAPbBr_3$/BCP[e]/LiF/Al	530	–	0.17	676	–	–	[55]
PET/SOCP/$MAPbBr_3$/TPBi/LiF/Al	~540	8.53	42.9	~10,000	–	–	[56]
PI/ITO/PEDOT:PSS/poly-TPD/$FAPbBr_3$/PMMA/3TPYMB/LiF/Al	530	2.0	8.4	~1000	2	–	[73]
PI/AgNWs/PEDOT:PSS/poly-TPD/perovskite/TPBi/Al/C protection layer	~750	13	–	–	2	–	[76]
Al/Al_2O_3/$CsPbBr_3$ QWs/NiO_x/IZO	520	7.3	22	31,667	–	–	[77]
VHB[f]/PI/AgNWs/PEDOT:PSS/TAPC:PVK[g]/perovskite QDs/TPBi/CsF/Al	532	–	9.2	3187	–	50%	[86]
Polymer/AgNWs/PEDOT:PSS/PVK:TAPC/$MAPbBr_3$/TmPyPB[h]/CsF/Al	521	2.6	10.4	1000	4	–	[88]
PET/ITO/NiO_x/perovskite/TPBi/LiF/Al	516	7.1	–	~12,000	–	–	[97]
PET/PVK/$CsPbBr_3$/$CsPb_2Br_3$/TPBi/LiF/Al	~515	0.3	–	904	–	–	[100]
PET/PDZ/$MAPbBr_3$/SPW-111/PFN/AgNWs	550	0.17	0.79	1260	2.5	–	[106]
PEN/ITO/PEDOT:PSS/perovskite/B3PyMPM[i]/LiF/Al	932	5.4	–	–	~2	–	[108]
PEN/ITO/TB(MA)/perovskite/TPBi/LiF/Al	488	8.3	14.7	2967	–	–	[117]
NOA 63[j]/Zonyl-PEDOT:PSS/perovskite/TPBi/LiF/Al	532	3.98	17.9	1060	2.5	–	[124]
PET/ITO/PEDOT:PSS/perovskite/TPBi/LiF/Al	529	5.9	25.1	3900	–	–	[123]
Graphene/PEDOT:PSS/poly-TPD/$FACsPbBr_3$/TPBi/LiF/Al	532	2.58	11.37	5358	–	–	[143]
PET/AnoHTL/$MAPbBr_3$/TPBi/LiF/Al	~540	8.66	42	~11,000	–	–	[144]
PU/PEDOT:PSS-PEO/PVP/$CsPbBr_3$-PEO-PVP[k]/PU-AgNWs	524	~0.27	380.5	1258	5	–	[151]
Ag-photopolymer/ZnO/PEI/$CsPbI_3$/TCTA[l]/MoO_3/Au/MoO_3	692	8.2	0.8	827	–	–	[152]
PET/ITO/PEDOT:PSS/$MAPbBr_3$/TPBi/AgNWs	~550	~0.04	657	180	–	–	[154]
PET/ITO/PEDOT:PSS/perovskite-PEG/ZnO/SMF[m]	533	4.6	22.3	98,000	–	–	[155]
PET/ITO/PEDOT:PSS/perovskite/PEDOT:PSS/LiF/Al	520	1.35	–	~10,000	–	–	[156]
PET/PDMS/PEDOT:PSS/PEO/perovskite/PEO/PEI/AgNWs	535	0.416	2.01	10,227	2.5	–	[157]

a) PEIE: ethoxylated-polyethylenimine; b) HATCN: 1,4,5,8,9,11-hexaazatriphenylene-hexanitrile; c) TAPC: hexachlorocyclotriphosphazene; d) PO-T2T: (1,3,5-triazine-2,4,6-triyl)tris(benzene-3,1-diyl)tris(diphenylphosphineoxide); e) BCP: bathocuproine; f) VHB: very high bond; g) PVK: poly(*N*-vinylcarbazole); h) TmPyPB: 1,3,5-tri(*m*-pyrid-3-yl-phenyl) benzene; i) B3PyMPM: 4,6-bis (3,5-di(pyridin-3-yl)phenyl)-2-methylpyrimidine; j) NOA 63: norland optical adhesive 63; k) PVP: polyvinylpyrrolidone; l) TCTA: 4,4′,4″-tri(*N*-carbazolyl)triphenylamine; m) SMF: silver microflake.

large-area thin films with high uniformity. Therefore, more efforts should be focused on the exploration of low-cost, flexible, and mass production fabrication techniques, such as compatible all-vacuum thermal evaporation and roll-to-roll (R2R) fabrication techniques (e.g., blade coating, spray coating, and inkjet printing) [179–181]. Tang and co-workers [97,182] successfully fabricated flexible green PeLEDs by an all-vacuum evaporation method with an area of 40.2 cm^2 and a favorable EQE of 7.1%, which is the best performance as far as we know. In addition, the EQEs of flexible PeLEDs prepared with the R2R techniques were not satisfactory and still lower than 4% [49,157,183]. Therefore, it has become imperative to develop compatible manufacturing techniques for large-scale flexible PeLEDs such as the R2R fabrication method to promote the commercial application of the flexible PeLEDs.

PERSPECTIVE

Buoyed by the remarkable optoelectronic and mechanical properties of MHPs, plenty of research has been conducted to explore the feasibility of flexible PeLEDs, in the hope of integrating them with wearable and portable optoelectronic devices and promoting the development of the next generation of flexible lighting and displays. For high-performance flexible PeLEDs, every single functional layer should have excellent functionality and flexibility to make the whole device with high efficiency and good operational stability. Therefore, proper optimization of each functional layer is required. Based on this, we propose some perspectives for the optimization of different functional layers, aiming to facilitate the development of flexible PeLEDs in the future.

(1) The properties of the perovskite emitting layers principally

determine the luminescent performance and operating stability of the flexible PeLEDs. In order to improve the properties of the perovskite emitters, sufficient attention should be paid to effective surface passivation, grain size engineering, and low dimensional engineering. Meanwhile, high-quality perovskite films are the prerequisite for achieving highly flexible and high-performance PeLEDs. Therefore, better preparation techniques for MHPs are also necessary.

(2) Ideal charge transporting layers could facilitate charge injection and block opposite carriers. The optimization of ETLs and HTLs should focus on the reduction of the charge injection potential barrier and the exciton quenching, as well as optimizing the interfacial contacts.

(3) Flexible transparent electrodes and substrates determine the bending properties and mechanical capability of flexible PeLEDs. Therefore, chemists and materials scientists should make concerted efforts to develop more novel materials suitable for highly flexible and highly conductive electrodes and substrates in the future.

(4) Compared with the relatively mature technology and mechanism of rigid PeLEDs, flexible PeLEDs face more challenges, especially the degradation of the performance including the luminescent stability and EQE in the bent or stretched state. Therefore, it is important to exploit new methods to improve the flexibility, stability, and adhesion between functional layers. In addition to improving the film morphology and developing ideal charge-transporting materials, the search for suitable stress-release materials and the synthesis of perovskites with flexural resistance structures are expected to solve this attractive problem [108,162].

CONCLUSION

In conclusion, we have comprehensively summarized the recent progress in the realm of flexible PeLEDs from the perspective of the optimization strategies of various functional layers based on previous outstanding research results. In addition, the major obstacles impeding the development of flexible PeLEDs in terms of stability, mechanical robustness, optical color balance, toxicity, and large-area fabrication, are discussed. Finally, the prospects for the development of flexible PeLEDs were foreseen. In view of the flourishing and encouraging research status in the field of flexible PeLEDs and the growing demand for high-quality displays and lighting, we believe that the flexible PeLEDs will show great potential for applications in the next-generation displays and lighting markets.

Received 5 May 2022; accepted 19 July 2022; published online 19 October 2022

1 Kim YH, Cho H, Lee TW. Metal halide perovskite light emitters. Proc Natl Acad Sci USA, 2016, 113: 11694–11702
2 Liu XK, Xu W, Bai S, *et al.* Metal halide perovskites for light-emitting diodes. Nat Mater, 2021, 20: 10–21
3 Sutherland BR, Sargent EH. Perovskite photonic sources. Nat Photon, 2016, 10: 295–302
4 Service RF. Perovskite LEDs begin to shine. Science, 2019, 364: 918
5 Tan ZK, Moghaddam RS, Lai ML, *et al.* Bright light-emitting diodes based on organometal halide perovskite. Nat Nanotech, 2014, 9: 687–692
6 Chu Z, Ye Q, Zhao Y, *et al.* Perovskite light-emitting diodes with external quantum efficiency exceeding 22% *via* small-molecule passivation. Adv Mater, 2021, 33: 2007169
7 Ma D, Lin K, Dong Y, *et al.* Distribution control enables efficient reduced-dimensional perovskite LEDs. Nature, 2021, 599: 594–598
8 Lin K, Xing J, Quan LN, *et al.* Perovskite light-emitting diodes with external quantum efficiency exceeding 20 percent. Nature, 2018, 562: 245–248
9 Cao Y, Wang N, Tian H, *et al.* Perovskite light-emitting diodes based on spontaneously formed submicrometre-scale structures. Nature, 2018, 562: 249–253
10 Liu Y, Dong Y, Zhu T, *et al.* Bright and stable light-emitting diodes based on perovskite quantum dots in perovskite matrix. J Am Chem Soc, 2021, 143: 15606–15615
11 Liu Z, Qiu W, Peng X, *et al.* Perovskite light-emitting diodes with EQE exceeding 28% through a synergetic dual-additive strategy for defect passivation and nanostructure regulation. Adv Mater, 2021, 33: 2103268
12 Yuan Z, Miao Y, Hu Z, *et al.* Unveiling the synergistic effect of precursor stoichiometry and interfacial reactions for perovskite light-emitting diodes. Nat Commun, 2019, 10: 2818
13 Jia P, Lu M, Sun S, *et al.* Recent advances in flexible perovskite light-emitting diodes. Adv Mater Interfaces, 2021, 8: 2100441
14 Chen H, Wang H, Wu J, *et al.* Flexible optoelectronic devices based on metal halide perovskites. Nano Res, 2020, 13: 1997–2018
15 Feng J. Mechanical properties of hybrid organic-inorganic $CH_3NH_3BX_3$ (B = Sn, Pb; X = Br, I) perovskites for solar cell absorbers. APL Mater, 2014, 2: 081801
16 Kim YH, Cho H, Heo JH, *et al.* Multicolored organic/inorganic hybrid perovskite light-emitting diodes. Adv Mater, 2015, 27: 1248–1254
17 Seo HK, Kim H, Lee J, *et al.* Efficient flexible organic/inorganic hybrid perovskite light-emitting diodes based on graphene anode. Adv Mater, 2017, 29: 1605587
18 Cheng LP, Huang JS, Shen Y, *et al.* Efficient $CsPbBr_3$ perovskite light-emitting diodes enabled by synergetic morphology control. Adv Opt Mater, 2018, 7: 1801534
19 Zhao X, Tan ZK. Large-area near-infrared perovskite light-emitting diodes. Nat Photonics, 2020, 14: 215–218
20 Shen Y, Li MN, Li Y, *et al.* Rational interface engineering for efficient flexible perovskite light-emitting diodes. ACS Nano, 2020, 14: 6107–6116
21 Veldhuis SA, Boix PP, Yantara N, *et al.* Perovskite materials for light-emitting diodes and lasers. Adv Mater, 2016, 28: 6804–6834
22 Zhao H, Liu G, Zhang J, *et al.* Analysis of internal quantum efficiency and current injection efficiency in III-nitride light-emitting diodes. J Display Technol, 2013, 9: 212–225
23 Protesescu L, Yakunin S, Bodnarchuk MI, *et al.* Nanocrystals of cesium lead halide perovskites ($CsPbX_3$, X = Cl, Br, and I): Novel optoelectronic materials showing bright emission with wide color gamut. Nano Lett, 2015, 15: 3692–3696
24 Ravi VK, Markad GB, Nag A. Band edge energies and excitonic transition probabilities of colloidal $CsPbX_3$ (X = Cl, Br, I) perovskite nanocrystals. ACS Energy Lett, 2016, 1: 665–671
25 Stranks SD, Snaith HJ. Metal-halide perovskites for photovoltaic and light-emitting devices. Nat Nanotech, 2015, 10: 391–402
26 Quan LN, Rand BP, Friend RH, *et al.* Perovskites for next-generation optical sources. Chem Rev, 2019, 119: 7444–7477
27 Goldschmidt VM. Die gesetze der krystallochemie. Naturwissenschaften, 1926, 14: 477–485
28 Green MA, Ho-Baillie A, Snaith HJ. The emergence of perovskite solar cells. Nat Photon, 2014, 8: 506–514
29 Yang WF, Igbari F, Lou YH, *et al.* Tin halide perovskites: Progress and challenges. Adv Energy Mater, 2019, 10: 1902584
30 Jang DM, Park K, Kim DH, *et al.* Reversible halide exchange reaction of organometal trihalide perovskite colloidal nanocrystals for full-range band gap tuning. Nano Lett, 2015, 15: 5191–5199
31 Manser JS, Christians JA, Kamat PV. Intriguing optoelectronic properties of metal halide perovskites. Chem Rev, 2016, 116: 12956–13008
32 Umebayashi T, Asai K, Kondo T, *et al.* Electronic structures of lead iodide based low-dimensional crystals. Phys Rev B, 2003, 67: 155405
33 Brandt RE, Stevanović V, Ginley DS, *et al.* Identifying defect-tolerant semiconductors with high minority-carrier lifetimes: Beyond hybrid

lead halide perovskites. MRS Commun, 2015, 5: 265–275
34 Zou Y, Cai L, Song T, *et al.* Recent progress on patterning strategies for perovskite light-emitting diodes toward a full-color display prototype. Small Sci, 2021, 1: 2000050
35 Wang N, Cheng L, Ge R, *et al.* Perovskite light-emitting diodes based on solution-processed self-organized multiple quantum wells. Nat Photon, 2016, 10: 699–704
36 Braly IL, deQuilettes DW, Pazos-Outón LM, *et al.* Hybrid perovskite films approaching the radiative limit with over 90% photoluminescence quantum efficiency. Nat Photon, 2018, 12: 355–361
37 Xiao P, Yu Y, Cheng J, *et al.* Advances in perovskite light-emitting diodes possessing improved lifetime. Nanomaterials, 2021, 11: 103
38 Lim KG, Han TH, Lee TW. Engineering electrodes and metal halide perovskite materials for flexible/stretchable perovskite solar cells and light-emitting diodes. Energy Environ Sci, 2021, 14: 2009–2035
39 Fang Y, Dong Q, Shao Y, *et al.* Highly narrowband perovskite single-crystal photodetectors enabled by surface-charge recombination. Nat Photon, 2015, 9: 679–686
40 Rakita Y, Cohen SR, Kedem NK, *et al.* Mechanical properties of $APbX_3$ (A = Cs or CH_3NH_3; X = I or Br) perovskite single crystals. MRS Commun, 2015, 5: 623–629
41 Reyes-Martinez MA, Abdelhady AL, Saidaminov MI, *et al.* Time-dependent mechanical response of $APbX_3$ (A = Cs, CH_3NH_3; X = I, Br) single crystals. Adv Mater, 2017, 29: 1606556
42 Sun S, Isikgor FH, Deng Z, *et al.* Factors influencing the mechanical properties of formamidinium lead halides and related hybrid perovskites. ChemSusChem, 2017, 10: 3740–3745
43 Yu J, Wang M, Lin S. Probing the soft and nanoductile mechanical nature of single and polycrystalline organic-inorganic hybrid perovskites for flexible functional devices. ACS Nano, 2016, 10: 11044–11057
44 Yang D, Zhao B, Yang T, *et al.* Toward stable and efficient perovskite light-emitting diodes. Adv Funct Mater, 2022, 32: 2109495
45 Adjokatse S, Fang HH, Loi MA. Broadly tunable metal halide perovskites for solid-state light-emission applications. Mater Today, 2017, 20: 413–424
46 Zheng W, Lin R, Zhang Z, *et al.* An ultrafast-temporally-responsive flexible photodetector with high sensitivity based on high-crystallinity organic-inorganic perovskite nanoflake. Nanoscale, 2017, 9: 12718–12726
47 Kim TH, Lee CS, Kim S, *et al.* Fully stretchable optoelectronic sensors based on colloidal quantum dots for sensing photoplethysmographic signals. ACS Nano, 2017, 11: 5992–6003
48 Chou SY, Ma R, Li Y, *et al.* Transparent perovskite light-emitting touch-responsive device. ACS Nano, 2017, 11: 11368–11375
49 Bade SGR, Li J, Shan X, *et al.* Fully printed halide perovskite light-emitting diodes with silver nanowire electrodes. ACS Nano, 2015, 10: 1795–1801
50 Yu JC, Park JH, Lee SY, *et al.* Effect of perovskite film morphology on device performance of perovskite light-emitting diodes. Nanoscale, 2019, 11: 1505–1514
51 Wang J, Wang N, Jin Y, *et al.* Interfacial control toward efficient and low-voltage perovskite light-emitting diodes. Adv Mater, 2015, 27: 2311–2316
52 Yu JC, Kim DB, Jung ED, *et al.* High-performance perovskite light-emitting diodes *via* morphological control of perovskite films. Nanoscale, 2016, 8: 7036–7042
53 Yu JC, Lee AY, Kim DB, *et al.* Enhancing the performance and stability of perovskite nanocrystal light-emitting diodes with a polymer matrix. Adv Mater Technol, 2017, 2: 1700003
54 Chen C, Han TH, Tan S, *et al.* Efficient flexible inorganic perovskite light-emitting diodes fabricated with $CsPbBr_3$ emitters prepared *via* low-temperature *in situ* dynamic thermal crystallization. Nano Lett, 2020, 20: 4673–4680
55 Jung DH, Park JH, Lee HE, *et al.* Flash-induced ultrafast recrystallization of perovskite for flexible light-emitting diodes. Nano Energy, 2019, 61: 236–244
56 Cho H, Jeong SH, Park MH, *et al.* Overcoming the electroluminescence efficiency limitations of perovskite light-emitting diodes. Science, 2015, 350: 1222–1225
57 Yang X, Zhang X, Deng J, *et al.* Efficient green light-emitting diodes based on quasi-two-dimensional composition and phase engineered perovskite with surface passivation. Nat Commun, 2018, 9: 570
58 Song L, Guo X, Hu Y, *et al.* Efficient inorganic perovskite light-emitting diodes with polyethylene glycol passivated ultrathin $CsPbBr_3$ films. J Phys Chem Lett, 2017, 8: 4148–4154
59 Dulkeith E, Ringler M, Klar TA, *et al.* Gold nanoparticles quench fluorescence by phase induced radiative rate suppression. Nano Lett, 2005, 5: 585–589
60 Samiee M, Konduri S, Ganapathy B, *et al.* Defect density and dielectric constant in perovskite solar cells. Appl Phys Lett, 2014, 105: 153502
61 Miyata A, Mitioglu A, Plochocka P, *et al.* Direct measurement of the exciton binding energy and effective masses for charge carriers in organic-inorganic tri-halide perovskites. Nat Phys, 2015, 11: 582–587
62 Xing G, Mathews N, Sun S, *et al.* Long-range balanced electron- and hole-transport lengths in organic-inorganic $CH_3NH_3PbI_3$. Science, 2013, 342: 344–347
63 Kavanagh LD, Schardt AW, Roelof EC. Quasi-two-dimensional perovskite light emitting diodes for bright future. Light Sci Appl, 2021, 10: 86
64 Han TH, Lee JW, Choi YJ, *et al.* Surface-2D/bulk-3D heterophased perovskite nanograins for long-term-stable light-emitting diodes. Adv Mater, 2020, 32: 1905674
65 Zhang L, Sun C, He T, *et al.* High-performance quasi-2D perovskite light-emitting diodes: From materials to devices. Light Sci Appl, 2021, 10: 61
66 Zhang J, Wang L, Zhang X, *et al.* Blue light-emitting diodes based on halide perovskites: Recent advances and strategies. Mater Today, 2021, 51: 222–246
67 Kumagai M, Takagahara T. Excitonic and nonlinear-optical properties of dielectric quantum-well structures. Phys Rev B, 1989, 40: 12359–12381
68 Zhang S, Yi C, Wang N, *et al.* Efficient red perovskite light-emitting diodes based on solution-processed multiple quantum wells. Adv Mater, 2017, 29: 1606600
69 Yuan M, Quan LN, Comin R, *et al.* Perovskite energy funnels for efficient light-emitting diodes. Nat Nanotech, 2016, 11: 872–877
70 Quan LN, Yuan M, Comin R, *et al.* Ligand-stabilized reduced-dimensionality perovskites. J Am Chem Soc, 2016, 138: 2649–2655
71 Dai X, Zhang Z, Jin Y, *et al.* Solution-processed, high-performance light-emitting diodes based on quantum dots. Nature, 2014, 515: 96–99
72 Liang D, Peng Y, Fu Y, *et al.* Color-pure violet-light-emitting diodes based on layered lead halide perovskite nanoplates. ACS Nano, 2016, 10: 6897–6904
73 Kumar S, Jagielski J, Kallikounis N, *et al.* Ultrapure green light-emitting diodes using two-dimensional formamidinium perovskites: Achieving recommendation 2020 color coordinates. Nano Lett, 2017, 17: 5277–5284
74 Kim YH, Kim S, Kakekhani A, *et al.* Comprehensive defect suppression in perovskite nanocrystals for high-efficiency light-emitting diodes. Nat Photonics, 2021, 15: 148–155
75 Miao Y, Cheng L, Zou W, *et al.* Microcavity top-emission perovskite light-emitting diodes. Light Sci Appl, 2020, 9: 89
76 Zhao L, Rolston N, Lee KM, *et al.* Influence of bulky organo-ammonium halide additive choice on the flexibility and efficiency of perovskite light-emitting devices. Adv Funct Mater, 2018, 28: 1802060
77 Zhang D, Zhang Q, Ren B, *et al.* Large-scale planar and spherical light-emitting diodes based on arrays of perovskite quantum wires. Nat Photon, 2022, 16: 284–290
78 Richter JM, Abdi-Jalebi M, Sadhanala A, *et al.* Enhancing photoluminescence yields in lead halide perovskites by photon recycling and light out-coupling. Nat Commun, 2016, 7: 13941
79 Kam M, Zhu Y, Zhang D, *et al.* Efficient mixed-cation mixed-halide perovskite solar cells by all-vacuum sequential deposition using metal oxide electron transport layer. Sol RRL, 2019, 3: 1900050
80 Li J, Yu Q, Gan L, *et al.* Perovskite light-emitting devices with a metal-insulator-semiconductor structure and carrier tunnelling. J Mater

Chem C, 2017, 5: 7715–7719
81 Xu L, Li J, Cai B, *et al.* A bilateral interfacial passivation strategy promoting efficiency and stability of perovskite quantum dot light-emitting diodes. Nat Commun, 2020, 11: 3902
82 Koscher BA, Swabeck JK, Bronstein ND, *et al.* Essentially trap-free $CsPbBr_3$ colloidal nanocrystals by postsynthetic thiocyanate surface treatment. J Am Chem Soc, 2017, 139: 6566–6569
83 Liu F, Zhang Y, Ding C, *et al.* Highly luminescent phase-stable $CsPbI_3$ perovskite quantum dots achieving near 100% absolute photoluminescence quantum yield. ACS Nano, 2017, 11: 10373–10383
84 Song J, Li J, Li X, *et al.* Quantum dot light-emitting diodes based on inorganic perovskite cesium lead halides ($CsPbX_3$). Adv Mater, 2015, 27: 7162–7167
85 Shi J, Li F, Jin Y, *et al. In situ* ligand bonding management of $CsPbI_3$ perovskite quantum dots enables high-performance photovoltaics and red light-emitting diodes. Angew Chem, 2020, 132: 22414–22421
86 Li YF, Chou SY, Huang P, *et al.* Stretchable organometal-halide-perovskite quantum-dot light-emitting diodes. Adv Mater, 2019, 31: 1807516
87 Wang HC, Bao Z, Tsai HY, *et al.* Perovskite quantum dots and their application in light-emitting diodes. Small, 2018, 14: 1702433
88 Zhao F, Chen D, Chang S, *et al.* Highly flexible organometal halide perovskite quantum dot based light-emitting diodes on a silver nanowire-polymer composite electrode. J Mater Chem C, 2017, 5: 531–538
89 Hu L, Zhao Q, Huang S, *et al.* Flexible and efficient perovskite quantum dot solar cells *via* hybrid interfacial architecture. Nat Commun, 2021, 12: 466
90 Liu J, Shabbir B, Wang C, *et al.* Flexible, printable soft-X-ray detectors based on all-inorganic perovskite quantum dots. Adv Mater, 2019, 31: 1901644
91 Li YF, Feng J, Sun HB. Perovskite quantum dots for light-emitting devices. Nanoscale, 2019, 11: 19119–19139
92 Dong Y, Wang YK, Yuan F, *et al.* Bipolar-shell resurfacing for blue LEDs based on strongly confined perovskite quantum dots. Nat Nanotechnol, 2020, 15: 668–674
93 Chiba T, Hayashi Y, Ebe H, *et al.* Anion-exchange red perovskite quantum dots with ammonium iodine salts for highly efficient light-emitting devices. Nat Photon, 2018, 12: 681–687
94 Liu Y, Li Z, Xu J, *et al.* Wide-bandgap perovskite quantum dots in perovskite matrix for sky-blue light-emitting diodes. J Am Chem Soc, 2022, 144: 4009–4016
95 Huang H, Zhao F, Liu L, *et al.* Emulsion synthesis of size-tunable $CH_3NH_3PbBr_3$ quantum dots: An alternative route toward efficient light-emitting diodes. ACS Appl Mater Interfaces, 2015, 7: 28128–28133
96 Li Y, Lv Y, Guo Z, *et al.* One-step preparation of long-term stable and flexible $CsPbBr_3$ perovskite quantum dots/ethylene vinyl acetate copolymer composite films for white light-emitting diodes. ACS Appl Mater Interfaces, 2018, 10: 15888–15894
97 Du P, Li J, Wang L, *et al.* Efficient and large-area all vacuum-deposited perovskite light-emitting diodes *via* spatial confinement. Nat Commun, 2021, 12: 4751
98 Peng X, Schlamp MC, Kadavanich AV, *et al.* Epitaxial growth of highly luminescent CdSe/CdS core/shell nanocrystals with photostability and electronic accessibility. J Am Chem Soc, 1997, 119: 7019–7029
99 Xu J, Huang W, Li P, *et al.* Imbedded nanocrystals of $CsPbBr_3$ in Cs_4PbBr_6: Kinetics, enhanced oscillator strength, and application in light-emitting diodes. Adv Mater, 2017, 29: 1703703
100 Tan Y, Li R, Xu H, *et al.* Ultrastable and reversible fluorescent perovskite films used for flexible instantaneous display. Adv Funct Mater, 2019, 29: 1900730
101 Quan LN, Quintero-Bermudez R, Voznyy O, *et al.* Highly emissive green perovskite nanocrystals in a solid state crystalline matrix. Adv Mater, 2017, 29: 1605945
102 Chen Z, Li Z, Zhang C, *et al.* Recombination dynamics study on nanostructured perovskite light-emitting devices. Adv Mater, 2018, 30: 1801370
103 Yan F, Demir HV. Vacuum-evaporated lead halide perovskite LEDs. Opt Mater Express, 2022, 12: 256–271
104 Hu Y, Wang Q, Shi YL, *et al.* Vacuum-evaporated all-inorganic cesium lead bromine perovskites for high-performance light-emitting diodes. J Mater Chem C, 2017, 5: 8144–8149
105 Li J, Du P, Li S, *et al.* High-throughput combinatorial optimizations of perovskite light-emitting diodes based on all-vacuum deposition. Adv Funct Mater, 2019, 29: 1903607
106 Lee SY, Kim SH, Nam YS, *et al.* Flexibility of semitransparent perovskite light-emitting diodes investigated by tensile properties of the perovskite layer. Nano Lett, 2019, 19: 971–976
107 Rolston N, Printz AD, Tracy JM, *et al.* Effect of cation composition on the mechanical stability of perovskite solar cells. Adv Energy Mater, 2017, 8: 1702116
108 Lu J, Guan X, Li Y, *et al.* Dendritic $CsSnI_3$ for efficient and flexible near-infrared perovskite light-emitting diodes. Adv Mater, 2021, 33: 2104414
109 Chen Y, Sun Y, Peng J, *et al.* 2D Ruddlesden-Popper perovskites for optoelectronics. Adv Mater, 2018, 30: 1703487
110 Zhang Q, Zhang D, Fu Y, *et al.* Light out-coupling management in perovskite LEDs—What can we learn from the past? Adv Funct Mater, 2020, 30: 2002570
111 Stranks SD, Hoye RLZ, Di D, *et al.* The physics of light emission in halide perovskite devices. Adv Mater, 2019, 31: 1803336
112 Zhang Q, Tavakoli MM, Gu L, *et al.* Efficient metal halide perovskite light-emitting diodes with significantly improved light extraction on nanophotonic substrates. Nat Commun, 2019, 10: 727
113 Yang JP, Bao QY, Xu ZQ, *et al.* Light out-coupling enhancement of organic light-emitting devices with microlens array. Appl Phys Lett, 2010, 97: 223303
114 Reineke S, Lindner F, Schwartz G, *et al.* White organic light-emitting diodes with fluorescent tube efficiency. Nature, 2009, 459: 234–238
115 Jeon S, Zhao L, Jung YJ, *et al.* Perovskite light-emitting diodes with improved outcoupling using a high-index contrast nanoarray. Small, 2019, 15: 1900135
116 Shen Y, Cheng LP, Li YQ, *et al.* High-efficiency perovskite light-emitting diodes with synergetic outcoupling enhancement. Adv Mater, 2019, 31: 1901517
117 Liu Y, Zhang L, Chen S, *et al.* Water-soluble conjugated polyelectrolyte hole transporting layer for efficient sky-blue perovskite light-emitting diodes. Small, 2021, 17: 2101477
118 Groenendaal L, Jonas F, Freitag D, *et al.* Poly(3,4-ethylenedioxythiophene) and its derivatives: Past, present, and future. Adv Mater, 2000, 12: 481–494
119 Crispin X, Marciniak S, Osikowicz W, *et al.* Conductivity, morphology, interfacial chemistry, and stability of poly(3,4-ethylene dioxythiophene)-poly(styrene sulfonate): A photoelectron spectroscopy study. J Polym Sci B Polym Phys, 2003, 41: 2561–2583
120 Yang Y, Deng H, Fu Q. Recent progress on PEDOT:PSS based polymer blends and composites for flexible electronics and thermoelectric devices. Mater Chem Front, 2020, 4: 3130–3152
121 Wang Z, Li Z, Zhou D, *et al.* Low turn-on voltage perovskite light-emitting diodes with methanol treated PEDOT:PSS as hole transport layer. Appl Phys Lett, 2017, 111: 233304
122 Lee S, Kim DB, Hamilton I, *et al.* Control of interface defects for efficient and stable quasi-2D perovskite light-emitting diodes using nickel oxide hole injection layer. Adv Sci, 2018, 5: 1801350
123 Kim H, Ra HN, Kim JS, *et al.* Improved performance of flexible perovskite light-emitting diodes with modified PEDOT:PSS hole transport layer. J Industrial Eng Chem, 2020, 90: 117–121
124 Lee SY, Nam YS, Yu JC, *et al.* Highly efficient flexible perovskite light-emitting diodes using the modified PEDOT:PSS hole transport layer and polymer-silver nanowire composite electrode. ACS Appl Mater Interfaces, 2019, 11: 39274–39282
125 Tengstedt C, Osikowicz W, Salaneck WR, *et al.* Fermi-level pinning at conjugated polymer interfaces. Appl Phys Lett, 2006, 88: 053502
126 Tan ZK, Vaynzof Y, Credgington D, *et al. In-situ* switching from barrier-limited to ohmic anodes for efficient organic optoelectronics. Adv Funct Mater, 2014, 24: 3051–3058

127 Zeng J, Qi Y, Liu Y, *et al.* ZnO-based electron-transporting layers for perovskite light-emitting diodes: Controlling the interfacial reactions. J Phys Chem Lett, 2022, 13: 694–703
128 Li W, Xu YX, Wang D, *et al.* Inorganic perovskite light emitting diodes with ZnO as the electron transport layer by direct atomic layer deposition. Org Electron, 2018, 57: 60–67
129 Zhuang S, Ma X, Hu D, *et al.* Air-stable all inorganic green perovskite light emitting diodes based on ZnO/$CsPbBr_3$/NiO heterojunction structure. Ceramics Int, 2018, 44: 4685–4688
130 Qasim K, Wang B, Zhang Y, *et al.* Solution-processed extremely efficient multicolor perovskite light-emitting diodes utilizing doped electron transport layer. Adv Funct Mater, 2017, 27: 1606874
131 Tang C, Shen X, Wu X, *et al.* Optimizing the performance of perovskite nanocrystal LEDs utilizing cobalt doping on a ZnO electron transport layer. J Phys Chem Lett, 2021, 12: 10112–10119
132 Lu P, Wu J, Shen X, *et al.* ZnO-Ti_3C_2 MXene electron transport layer for high external quantum efficiency perovskite nanocrystal light-emitting diodes. Adv Sci, 2020, 7: 2001562
133 Liu B, Wang L, Gu H, *et al.* Highly efficient green light-emitting diodes from all-inorganic perovskite nanocrystals enabled by a new electron transport layer. Adv Opt Mater, 2018, 6: 1800220
134 Cai L, Yang F, Xu Y, *et al.* Dual functionalization of electron transport layer *via* tailoring molecular structure for high-performance perovskite light-emitting diodes. ACS Appl Mater Interfaces, 2020, 12: 37346–37353
135 Fang T, Wang T, Li X, *et al.* Perovskite QLED with an external quantum efficiency of over 21% by modulating electronic transport. Sci Bull, 2021, 66: 36–43
136 Sun S, Lu M, Guo J, *et al.* Double electron transport layer and optimized $CsPbI_3$ nanocrystal emitter for efficient perovskite light-emitting diodes. J Phys Chem C, 2020, 124: 28277–28284
137 Lee P, Lee J, Lee H, *et al.* Highly stretchable and highly conductive metal electrode by very long metal nanowire percolation network. Adv Mater, 2012, 24: 3326–3332
138 Park H, Rowehl JA, Kim KK, *et al.* Doped graphene electrodes for organic solar cells. Nanotechnology, 2010, 21: 505204
139 Eda G, Fanchini G, Chhowalla M. Large-area ultrathin films of reduced graphene oxide as a transparent and flexible electronic material. Nat Nanotech, 2008, 3: 270–274
140 Berger C, Song Z, Li X, *et al.* Electronic confinement and coherence in patterned epitaxial graphene. Science, 2006, 312: 1191–1196
141 Wu Z, Chen Z, Du X, *et al.* Transparent, conductive carbon nanotube films. Science, 2004, 305: 1273–1276
142 Zhang M, Fang S, Zakhidov AA, *et al.* Strong, transparent, multifunctional, carbon nanotube sheets. Science, 2005, 309: 1215–1219
143 Zhang Q, Lu Y, Liu Z, *et al.* Highly efficient organic-inorganic hybrid perovskite quantum dot/nanocrystal light-emitting diodes using graphene electrode and modified PEDOT:PSS. Org Electron, 2019, 72: 30–38
144 Jeong SH, Woo SH, Han TH, *et al.* Universal high work function flexible anode for simplified ITO-free organic and perovskite light-emitting diodes with ultra-high efficiency. NPG Asia Mater, 2017, 9: e411
145 Kim N, Kee S, Lee SH, *et al.* Highly conductive PEDOT:PSS nanofibrils induced by solution-processed crystallization. Adv Mater, 2014, 26: 2268–2272
146 Kirchmeyer S, Reuter K. Scientific importance, properties and growing applications of poly(3,4-ethylenedioxythiophene). J Mater Chem, 2005, 15: 2077
147 Kim GH, Shao L, Zhang K, *et al.* Engineered doping of organic semiconductors for enhanced thermoelectric efficiency. Nat Mater, 2013, 12: 719–723
148 Wegner G. Polymers with metal-like conductivity—A review of their synthesis, structure and properties. Angew Chem Int Ed Engl, 1981, 20: 361–381
149 Murgatroyd PN. Theory of space-charge-limited current enhanced by Frenkel effect. J Phys D-Appl Phys, 1970, 3: 151–156
150 Campbell IH, Smith DL, Neef CJ, *et al.* Consistent time-of-flight mobility measurements and polymer light-emitting diode current-voltage characteristics. Appl Phys Lett, 1999, 74: 2809–2811
151 Jiang DH, Liao YC, Cho CJ, *et al.* Facile fabrication of stretchable touch-responsive perovskite light-emitting diodes using robust stretchable composite electrodes. ACS Appl Mater Interfaces, 2020, 12: 14408–14415
152 Lu M, Wu H, Zhang X, *et al.* Highly flexible $CsPbI_3$ perovskite nanocrystal light-emitting diodes. ChemNanoMat, 2018, 5: 313–317
153 Li Y, Meng L, Yang YM, *et al.* High-efficiency robust perovskite solar cells on ultrathin flexible substrates. Nat Commun, 2016, 7: 10214
154 Kim T, Kim JH, Park JW. Semi-transparent organic-inorganic hybrid perovskite light-emitting diodes fabricated under high relative humidity. Solid-State Electron, 2020, 165: 107749
155 Payandeh M, Ahmadi V, Roghabadi FA, *et al.* High-brightness perovskite light-emitting diodes using a printable silver microflake contact. ACS Appl Mater Interfaces, 2020, 12: 11428–11437
156 Bi S, Zhao W, Sun Y, *et al.* Dynamic photonic perovskite light-emitting diodes with post-treatment-enhanced crystallization as writable and wipeable inscribers. Nanoscale Adv, 2021, 3: 6659–6668
157 Zhao J, Lo LW, Wan H, *et al.* High-speed fabrication of all-inkjet-printed organometallic halide perovskite light-emitting diodes on elastic substrates. Adv Mater, 2021, 33: 2102095
158 Fan Z, Chen Y, Lin Y, *et al.* Preface to the special issue on flexible energy devices. J Semicond, 2021, 42: 100101
159 Zou Y, Yuan Z, Bai S, *et al.* Recent progress toward perovskite light-emitting diodes with enhanced spectral and operational stability. Mater Today Nano, 2019, 5: 100028
160 Zhang D, Fu Y, Zhan H, *et al.* Suppressing thermal quenching *via* defect passivation for efficient quasi-2D perovskite light-emitting diodes. Light Sci Appl, 2022, 11: 69
161 Zhang J, Zhang W, Cheng HM, *et al.* Critical review of recent progress of flexible perovskite solar cells. Mater Today, 2020, 39: 66–88
162 Chen CH, Su ZH, Lou YH, *et al.* Full-dimensional grain boundary stress release for flexible perovskite indoor photovoltaics. Adv Mater, 2022, 34: 2200320
163 Zhang H, Rogers JA. Recent advances in flexible inorganic light emitting diodes: From materials design to integrated optoelectronic platforms. Adv Opt Mater, 2019, 7: 1800936
164 Hassan Y, Park JH, Crawford ML, *et al.* Ligand-engineered bandgap stability in mixed-halide perovskite LEDs. Nature, 2021, 591: 72–77
165 Zhang K, Zhu N, Zhang M, *et al.* Opportunities and challenges in perovskite LED commercialization. J Mater Chem C, 2021, 9: 3795–3799
166 Wang HC, Wang W, Tang AC, *et al.* High-performance $CsPb_{1-x}Sn_xBr_3$ perovskite quantum dots for light-emitting diodes. Angew Chem Int Ed, 2017, 56: 13650–13654
167 Qiu W, Xiao Z, Roh K, *et al.* Mixed lead-tin halide perovskites for efficient and wavelength-tunable near-infrared light-emitting diodes. Adv Mater, 2019, 31: 1806105
168 Lu M, Zhang X, Zhang Y, *et al.* Simultaneous strontium doping and chlorine surface passivation improve luminescence intensity and stability of $CsPbI_3$ nanocrystals enabling efficient light-emitting devices. Adv Mater, 2018, 30: 1804691
169 Yao JS, Ge J, Wang KH, *et al.* Few-nanometer-sized α-$CsPbI_3$ quantum dots enabled by strontium substitution and iodide passivation for efficient red-light emitting diodes. J Am Chem Soc, 2019, 141: 2069–2079
170 Lu M, Guo J, Sun S, *et al.* Bright $CsPbI_3$ perovskite quantum dot light-emitting diodes with top-emitting structure and a low efficiency roll-off realized by applying zirconium acetylacetonate surface modification. Nano Lett, 2020, 20: 2829–2836
171 Shen X, Zhang Y, Kershaw SV, *et al.* Zn-alloyed $CsPbI_3$ nanocrystals for highly efficient perovskite light-emitting devices. Nano Lett, 2019, 19: 1552–1559
172 Zou S, Liu Y, Li J, *et al.* Stabilizing cesium lead halide perovskite lattice through Mn(II) substitution for air-stable light-emitting diodes. J Am Chem Soc, 2017, 139: 11443–11450
173 Hou S, Gangishetty MK, Quan Q, *et al.* Efficient blue and white perovskite light-emitting diodes *via* manganese doping. Joule, 2018, 2: 2421–2433

174 Chen Z, Zhou B, Yuan J, *et al.* Cu^{2+}-doped $CsPbI_3$ nanocrystals with enhanced stability for light-emitting diodes. J Phys Chem Lett, 2021, 12: 3038–3045
175 Liu M, Jiang N, Huang H, *et al.* Ni^{2+}-doped $CsPbI_3$ perovskite nanocrystals with near-unity photoluminescence quantum yield and superior structure stability for red light-emitting devices. Chem Eng J, 2021, 413: 127547
176 Wang Q, Wang X, Yang Z, *et al.* Efficient sky-blue perovskite light-emitting diodes *via* photoluminescence enhancement. Nat Commun, 2019, 10: 5633
177 Yao JS, Ge J, Han BN, *et al.* Ce^{3+}-doping to modulate photoluminescence kinetics for efficient $CsPbBr_3$ nanocrystals based light-emitting diodes. J Am Chem Soc, 2018, 140: 3626–3634
178 Qiu L, Ono LK, Qi Y. Advances and challenges to the commercialization of organic-inorganic halide perovskite solar cell technology. Mater Today Energy, 2018, 7: 169–189
179 Tang G, Yan F. Flexible perovskite solar cells: Materials and devices. J Semicond, 2021, 42: 101606
180 Bhaumik S, Kar MR, Thorat BN, *et al.* Vacuum-processed metal halide perovskite light-emitting diodes: Prospects and challenges. ChemPlusChem, 2021, 86: 558–573
181 Howard IA, Abzieher T, Hossain IM, *et al.* Coated and printed perovskites for photovoltaic applications. Adv Mater, 2019, 31: 1806702
182 Du P, Gao L, Tang J. Focus on performance of perovskite light-emitting diodes. Front Optoelectron, 2020, 13: 235–245
183 Wang J, Li D, Mu L, *et al.* Inkjet-printed full-color matrix quasi-two-dimensional perovskite light-emitting diodes. ACS Appl Mater Interfaces, 2021, 13: 41773–41781

Acknowledgements This work was supported by the National Natural Science Foundation of China (52073197 and 62075148), the Natural Science Foundation of Jiangsu Province (BK20201413 and BK20211314), Suzhou Key Laboratory of Functional Nano & Soft Materials, Collaborative Innovation Center of Suzhou Nano Science & Technology, the 111 Project, the Joint International Research Laboratory of Carbon-Based Functional Materials and Devices, and Soochow University Tang Scholar.

Author contributions Wang JT and Wang ZK conceived the idea for this review. Wang JT collected the references, organized the images, and wrote the entire manuscript; Wang SZ, Zhou YH, and Lou YH modified the manuscript and participated in the discussion; all the authors contributed to the general discussion. Lou YH and Wang ZK supervised the project.

Conflict of interest The authors declare that they have no conflict of interest.

Jin-Tao Wang is pursuing his bachelor of engineering degree at the College of Nano Science & Technology (CNST), Soochow University, China. In 2020, he joined the research group of Prof. Zhao-Kui Wang as an undergraduate trainee for scientific research training at the Institute of Functional Nano & Soft Materials (FUNSOM), Soochow University. His primary research interest is perovskite light-emitting diodes.

Yan-Hui Lou received her PhD degree in nano and novel matter science from the University of Toyama, Japan, in 2012. After working at the University of Toyama as a Japan Society for the Promotion of Science (JSPS) research fellow from 2012 to 2014, she joined Soochow Institute for Energy and Materials Innovations, Soochow University, as an associate professor. Since 2021, she has been a full professor at Soochow University. Her main research interest focuses on organic and inorganic/organic hybrid materials for application in solar cells.

Zhao-Kui Wang received his PhD degree in nano and novel matter science from the University of Toyama, Japan, in 2011. After working at the University of Toyama as a JSPS research fellow from 2011 to 2013, he joined the Institute of FUNSOM, Soochow University, as an associate professor. Since 2017, he has been a full professor at Soochow University. His main research interests lie in organic and inorganic/organic hybrid materials and devices, focusing on solar cells and light-emitting diodes (LEDs).

柔性钙钛矿发光二极管: 进展, 挑战与展望

王金涛[1], 王树状[1], 周宇航[1], 娄艳辉[2*], 王照奎[1*]

摘要 金属卤化物钙钛矿具有优异的光电性能和良好的延展性, 是一种很有前途的适合于柔性光电子器件的材料, 并且可以集成到便携式和可穿戴式的显示设备中, 在下一代显示和照明方面展现出巨大的潜力. 目前, 柔性钙钛矿发光二极管领域已经取得了令人鼓舞的进展, 最大外量子效率已经超过28%. 在此, 我们总结了近年来在柔性钙钛矿发光二极管领域取得的主要突破, 旨在提供一个全面的回顾, 以促进柔性钙钛矿发光二极管的进一步发展. 此外, 我们还讨论了阻碍柔性钙钛矿发光二极管器件性能和商业化的主要挑战. 最后, 我们对柔性钙钛矿发光二极管的未来机遇和应用前景进行了展望和总结.

